The Use of Series Compliance and Variable Transmission Elements in the Design of a Powered Knee Prosthesis

by

Luke Matthewson Mooney

S.B. Mechanical Engineering, Massachusetts Institute of Technology (2012)

Submitted to the Department of Mechanical Engineering in partial fulfillment of the requirements for the degree of

Master of Science

at the

MASSACHUSETTS INSTITUTE OF TECHNOLOGY

June 2014

Signature redacted

Author .....
Department of Mechanical Engineering
May 7, 2012

Signature redacted

Certified by ....
Hugh M. Herr
Associate Professor, Media Arts and Sciences
Thesis Supervisor

Signature redacted

Certified by ....
Amos Winter
Assistant Professor, Department of Mechanical Engineering
Thesis Reader

Signature redacted

Accepted by ....
David E. Hardt
Ralph E. and Eloise F. Cross Professor of Mechanical Engineering
Graduate Officer, Department of Mechanical Engineering

The Use of Series Compliance and Variable Transmission Elements in the Design of a Powered Knee Prosthesis

by

Luke Matthewson Mooney

Submitted to the Department of Mechanical Engineering
on May 16, 2012, in partial fulfillment of the
requirements for the degree of
Master of Science

Abstract

Compared to non-amputees, above knee amputees expend significantly more metabolic energy. This is a result of the passive nature of most knee prostheses, as the development of clinically successful powered knee prostheses has remained a challenge. The addition of powered elements, such as electric motors, allow prosthetic knees to more closely emulate natural knee biomechanics. However, the addition of powered elements presents a new challenge of creating energy efficient devices that do not require frequent charging or excessively large batteries. In this thesis, a general optimization routine was developed to simulate and evaluate the electrical economy of various actuator architectures. Advanced actuators utilizing variable transmissions with elastic elements were compared to direct drive actuators, series elastic actuators, and two novel mechanisms known as the continuously-variable series-elastic actuator (CV-SEA) and the clutchable series-elastic actuator (CSEA). The CV-SEA is similar to a traditional series-elastic actuator (SEA), but uses a controllable continuously-variable transmission (CVT) in between the series-elastic element and the motor. The CSEA included a low-power clutch in parallel with an electric motor within a traditional series-elastic actuator. The stiffness of the series elasticity was tuned to match the elastically conservative region of the knees torque-angle relationship during early stance phase knee flexion and extension. During this region of the gait cycle, the clutch was engaged and elastic energy was stored in the spring, thereby providing the reactionary torque at a substantially reduced electrical cost. The optimization routine showed that the electrical economy of knee prostheses can be greatly improved by implementing variable transmissions in series with elastic elements. The optimization routine also estimated that a CSEA knee prosthesis could provide an 83% reduction in electrical cost, when compared to an SEA knee prosthesis. Although the variable transmission actuators were predicted to be more electrically economical than the CSEA knee, their design complexity limits their current feasibility in a knee prosthesis. Thus, a fully autonomous knee prosthesis utilizing the CSEA was designed, developed and tested. The CSEA Knee was actuated with a brushless electric motor; ballscrew transmission and cable drive as well as commercial electrical components.

The knee was lighter than the 8th percentile and shorter than the 1st percentile male shank segment. The CSEA Knee was tested in a unilateral above knee amputee walking at 1.3 m/s. During walking, the CSEA Knee provided biomechanically-accurate torque-angle behavior, agreeing within 17% of the net work and 73% of the stance flexion angle produced by the biological knee during locomotion. Additionally, the process of locomotion reduced the net electrical energy consumed of the CSEA Knee. The knees motor generated 1.8 J/stride, while the electronics consumed 5.4 J/Stride. Thus the net energy consumption was 3.6 J/stride, an order of magnitude less electrical energy consumption than previously published powered knee prostheses. Future work will focus on a custom, power-optimized embedded system and the expansion of the CSEA architecture to other biomechanically relevant joints for bionic prosthesis development.

Thesis Supervisor: Hugh M. Herr
Title: Associate Professor, Media Arts and Sciences

Contents

List of Figures

Chapter 1

Introduction

Transfemoral, or above knee amputees, expend significantly more metabolic energy during walking than non-amputees (50-120% increase) [1]. Additionally, the majority of such amputees are dissatisfied with the extent they use their prostheses [2] and express lack of mobility as a chief concern [3]. There is a need to develop highly efficient, lightweight powered leg prostheses that are able to provide biologically equivalent joint kinetics and kinematics. Such devices have the potential to restore natural movement patterns and substantially impact quality of life for such individuals.

The passivity of many knee prostheses is one cause of their shortcomings. Specifically, these prostheses typically incorporate hydraulic, pneumatic or friction elements and are thought to be limited in their inability to accommodate varying walking speeds and early stance phase knee flexion. To address these limitations, quasi-passive knee prostheses use a microcontroller to vary the damping characteristics automatically throughout the gait cycle. Quasi-passive knees have been shown to increase self-selected walking speed as well as decrease peak vertical ground reaction force and metabolic cost, when compared to traditional passive knees [4, 5, 6, 7]. However, despite their benefits, neither passive nor quasi-passive knee prostheses can contribute net positive mechanical energy. Hence they cannot replicate the net positive power phases of the gait cycle, or assist in net-positive locomotion modes (i.e. stair or ramp ascent). Furthermore, extended use of these passive prostheses has been implicated in a number of gait asymmetries [8, 6], secondary disabilities as well as failing to reduce

the metabolic cost of locomotion to the level of non-amputees [9, 10].

Recent advancements in battery chemistry, brushless motor design and microprocessors have bolstered the development of autonomous and semi-autonomous powered prosthetic knees [11, 12, 13, 14, 15]. Sup et al. [11, 12] designed a powered knee and ankle prosthesis that used a finite-state impedance controller during locomotion, and more recently Ha et al. investigated volitional control of the same prosthesis using surface electromyography [16]. This research is encouraging; however, the design of this prosthesis has no inherent elasticity, and is therefore subject to shock loads during use and high electrical power consumption. Martinez-Villalpando et al. presented an Active Agonist-Antagonist Knee Prosthesis [13, 17, 15], where dual series elastic actuators actuated the knee joint in parallel to reduce the consumption of electrical energy. A variable impedance control scheme was shown qualitatively to replicate able-bodied kinematics [13], however, as a result of the dual, brushed actuators, improvements on the size, weight and efficiency of the prosthesis are limited. Lastly, Ossur has developed the Power Knee; however, this prosthesis has not been shown to provide substantial benefit to the intact limb [18]. Thus, despite promising previous work, the development of an energy efficient, series-elastic knee prosthesis remains a challenge.

Early stance knee flexion and extension, the phase of the knee angle profile following heel strike while bodyweight is borne by the leg, is an important portion of the gait cycle rarely seen in the gait of transfemoral amputees [4]. Early stance knee flexion is known to aid in shock absorption during heel contact [19], thereby reducing metabolic expenditure. The lack of this gait characteristic in transfemoral amputees may explain part of the increased metabolic cost of locomotion observed in this population. Thus, the development of future state-of-the-art robotic knee prostheses must be able to biomechanically replicate this important phase of locomotion.

The purpose of this thesis is to explore different electromechanical actuator architectures that could be used to reduce the electrical energetic cost of a robotic knee prosthesis. Different actuator architectures were explored and their electrical economy as knee prosthesis actuators were simulated. Advanced actuators utilizing

variable transmissions with elastic elements were compared to direct drive actuators, series elastic actuators, and two novel mechanisms known as the continuously-variable series-elastic actuator (CV-SEA), and the clutchable series-elastic actuator (CSEA). Although the variable transmission actuators were predicted to be more electrically economical than the CSEA knee, their design complexity limits their current feasibility in a knee prosthesis. Thus, a fully autonomous knee prosthesis utilizing the CSEA was designed, developed and tested.

Chapter 2

Robotic Actuators

The performance and energetic efficiency (electrical energy needed to perform a task) of actuating legged locomotion are important factors to consider when designing powered leg prostheses, orthoses, exoskeletons, and legged robots. The electrical energy required by a motorized legged robot can be reduced by choosing an actuator architecture that takes advantage of legged locomotion dynamics. Motors are most efficient when operating at intermediate speeds and low torque, but legged locomotion involves bidirectional joints operating at various speeds and torques [20]. Legged locomotion also includes periods of both negative and positive mechanical power [20], so an efficient actuator should be able to store elastic energy during periods of negative power, and release that energy during periods of positive power. Motors can act as generators, but the highest harvesting efficiency (ratio of stored electrical energy to mechanical human energy) is only 63 percent [21]. An efficient motorized actuator for legged robots would both operate the motor at low torques, where the motors is most efficient, and efficiently store elastic energy so as to mitigate actuator work requirements.

Over the past two decades, series-elastic actuators (SEAs) have been the focus of significant research in force controlled robots [22, 23, 24, 25, 26]. An SEA includes a series compliance between the transmission output and the load, which has been shown to have substantial advantages. Such advantages include an increase in shock tolerance, limited high-frequency actuator impedance, and elastic energy storage for

power amplification [22, 27]. Moreover, the series compliance increases force fidelity, a property especially useful in the impedance controlled applications in fields such as wearable robotics and human-machine interfacing [28, 29, 30].

SEAs have been previously implemented in lower extremity prosthetic and exoskeleton devices. Au et al. used series and parallel elasticity in the design of a powered ankle prosthesis [30], which was shown to lower the metabolic cost of walking in transtibial amputees [31]. Additionally, Veneman et al. [29] designed a lower extremity exoskeleton device using Bowden cable driven SEAs. Recently, a new iteration of the design was proposed that used a direct-mounted SEA rather than the Bowden cable drive [32]. As a result of the SEAs implemented in these designs, they have many favorable attributes; however, the cyclic and often spring-like torque-angle relationship observed during locomotion presents an opportunity to further innovate on the SEA architecture.

During the early stance knee flexion and extension phase of human locomotion the torque-angle relationship is linear, or spring-like [33]. An SEA implemented with a series stiffness approximately equal to the slope of this knee torque-angle relationship (often termed the quasi-stiffness [34]) would provide a reduction in the mechanical work required by the motor within the SEA. In other words, the complete torque-angle relationship would be rendered by the physical spring alone requiring only reactionary torque to be generated by the motor, at negligible motor speed and mechanical power. This provides a decrease in the mechanical energy required by the motor; however, because electric motors are inefficient at low speeds, an additional improvement may be made. In this investigation, we place a small clutch on the motor shaft to supply the reactionary torque on the motor's shaft when the actuator output dynamics are elastically conservative such as, for example, during the early stance knee flexion-extension phase of human walking.

Although having series compliance within an actuator has many benefits, series compliance alone limits a designer's capacity to fine tune motor operating speeds to optimize motor efficiency across a diverse set of actuator tasks. Forcing the motor to operate at extremes of motor speed results in a lower efficiency. Another approach to

increasing the efficiency of an actuator is to provide a means to vary the transmission ratio, so that the motor can operate efficiently at both high speed/lower torque output regimes and at low speed/high torque output regimes. Various forms of continuously variable transmissions (CVTs) have been explored [35, 36, 37]. CVTs can be divided into two major categories, those that passively control the transmission ratio by reacting to velocity or torque [36, 35], and those that have active control over the transmission ratio [37].

The passive control of CVTs eliminates the need to develop a control strategy for the transmission ratio, but it does not guarantee an energy efficient transmission profile. Researchers have developed passively controlled CVTs [36, 35]. Passively controlled CVTs can store some amount of energy, but the energy storage is a byproduct of the passive transmission ratio control. The energy storage is also coupled to both angle and torque, which limits the amount of energy that can be stored.

Actively controlling CVTs to reduce electrical energy requirements have also been investigated in multiple areas of research. Previous research has been conducted on the appropriate control of CVTs when implemented in automobiles [38], but these methods focused on unidirectional motion and thus do not efficiently translate to cyclic bidirectional motion. A controllable CVT for quadruped motion was also developed. The device used a crank-type CVT with two equivalent actuators and no elastic element [37]. The controllable CVT would allow a more energy efficient control strategy in principle, but the device did not provide a means for efficiently storing energy during negative power periods [37].

Infinitely variable transmissions (IVTs) have also been investigated. IVTs allow the input motor to run at a constant speed with the output producing a controllable velocity that can reverse directions. The active control of IVTs used in haptic devices has been extensively investigated [39, 40, 41, 42]. These haptic control strategies mention the possible energy advantages, but focus on expanding the dynamic range of the device. Similar to a CVT, an IVT reduces the load on the motor, but it also cannot store elastic energy. Any negative mechanical power must be transformed into electrical energy by the motor.

Recently, Stramigiolo et al. presented a new actuator, the Very Versatile Energy Efficient (V2E2) actuator which utilizes a parallel motor and clutch in series with an elastic element and IVT [43]. Both [43] and [44] suggest that this novel architecture could significantly reduce the energy consumption of locomotive robotics, but the control strategy is neither fully developed nor compared to any other architecture. The proposed IVT used in the V2E2 also exhibits low efficiencies as the transmission reverses direction [45, 46, 47], a frequent occurrence in legged robotics. These regions of IVT inefficiency increase the energy of replicating legged locomotion, and will be further discussed in the Methods section.

The capabilities of different variable stiffness actuators (VSAs) have been investigated by many groups [48]. A VSA can be constructed by placing a variable transmission between the output and an elastic element [48, 43]. The apparent stiffness of the elastic element is controlled by actuating the variable transmission. The VSA allows energy to be stored and released from the elastic element at varying stiffnesses. A VSA can mechanically store energy in the elastic element during different dynamic regimes, but this architecture forces the variable transmission to be in between the load and elastic element. Therefore, the variable transmission must be able to accommodate the full torque seen at the elastic element. Placing a constant transmission between the variable transmission and the load can reduce the torque seen by the elastic element. However, this arrangement increases the deflection of the elastic element for a given amount of energy storage, increasing the size of the device.

Previous work incorporating clutchable elements into wearable robotic actuators have been studied. Haeufle et al. [49] introduced a clutched parallel-elastic actuator. In their work, a spring was incorporated in parallel to the electric motor and was engaged via a clutch. The purpose of the parallel spring was to augment the torque angle characteristics of the mechanism passively. Such a design is advantageous because it enabled a reduced gear ratio and less powerful motor to be used, while maintaining the proper kinematics and kinetics of stance phase. However because there is no series compliance between the transmission output and the load, this mechanism cannot take advantage of the aforementioned beneficial properties of

an SEA. Furthermore, because human locomotion includes spontaneous high-power modes (e.g. stair ascent and sit-to-stand transitions), it is essential for a prosthesis to be able to provide significant output power. Thus, the potential clinical benefit provided by the parallel spring design is likely outweighed by its inability to provide a complete array of locomotory modes required during activities of daily living.

Chapter 3

Actuator Optimization Methods

3.1 Electric Motor Model

Since legged locomotion is typically a cyclic process, the efficiency of actuators was examined by enforcing a particular kinematic and kinetic output from a biological joint. First, a linear model of an electric motor was used to estimate the energy requirements of different transmissions and load scenarios. The voltage, V, and current, I of a motor driving a given dynamic trajectory were estimated by 3.1 and 3.2:

$$V = R_m I + k_b \dot{\theta}_m \tag{3.1}$$

$$I = \frac{J_m \ddot{\theta}_m + \tau_m + \nu_m \dot{\theta}_m}{k_t} \tag{3.2}$$

where R_m is the motors resistance, k_b is the back emf constant, k_t is the torque constant, J_m is the motors rotor inertia, ν_m is the damping coefficient of the motor, $\dot{\theta}_m$ and $\ddot{\theta}_m$ are the motors velocity and acceleration, and τ_m is the torque supplied by the motor.

Using 3.1 and 3.2 to estimate V and I, the power of the motor, p_m was defined as:

Table 3.1: Brushless motor Parameters

Parameter	Symbol	Value
Terminal Resistance	R_m	0.21Ω
Voltage Constant	k_b	$0.021 rad\, s^{-1} V^{-1}$
Rotor Inertia	J_m	$33x10^{-7}\, kg\, m^2$
Damping	ν_b	$5.7x10^{-6}\, Nm\, rad^{-1} s$
Torque Constant	k_t	$0.021 Nm\, A^{-1}$
Charging Efficiency	η_{gen}	0.5

$$p_m = \begin{cases} IV\eta_{act}^{-1} & \text{if } IV > 0, \\ IV\eta_{act}\eta_{gen} & \text{if } IV < 0, \end{cases} \tag{3.3}$$

where η_{act} is the efficiency of the actuator and η_{gen} is the efficiency of converting mechanical power into electrical power, which was conservatively set to 0.5 [21]. In order to account for inefficiencies in the actuator, η_{act} was defined as the ratio of the output mechanical power to the input mechanical power. Equation 3.3 shows that the required electrical power is divided by η_{act} when the actuator is providing positive power, and the electrical power is multiplied by η_{act} and η_{gen} when the electric motor is being used as a generator and charging the batteries. The motor inertia was assumed to be twice the value of the actual motor rotor inertia in order to account for the reflected inertia of the different transmission architectures. This is a limitation of the presented optimization, since different actuator architectures will likely result in different reflected inertias. Equations 3.1 and 3.2 combined with 3.3 estimate the electric power of the actuator given the dynamics of the motor.

A 36 V, 200 W brushless motor was used for all of the actuator optimizations (model: EC-30 4-pole, Maxon Motor, Sachseln, Switzerland). The EC-30 was chosen for its high specific power and efficiency, and is a standard choice in the field of powered prostheses [12]. The parameters of the brushless motor are shown in Trable 3.1;

3.2 Actuator Architectures and Dynamics

This thesis focuses on the optimization of the electrical energy consumed by a generalized actuator while performing the function of a powered knee prosthesis. The generalized actuator may be comprised of an electric motor, a variable CVT, an IVT, a series elastic element, and a constant transmission. It was assumed that the actuator will have at most one variable transmission (CVT or IVT), at most one series elastic element, and only one electric motor. Furthermore, the presented optimization is constrained to not include a constant transmission between the load and spring. This assumption is made because such a transmission effectively decreases the stiffness of the spring, which results in higher deflections to store an equivalent amounts of energy. Actuators for wearable devices are often limited by space and cannot accommodate large deflection springs. Given these constraints, the generalized actuator can be arranged in six configurations Fig. 3-1.

The dynamics of the electric motor were calculated as functions of the given load dynamics and transmission properties. Transmission ratios were defined as the ratio between input torque and output torque. Therefore, all transmission ratios were less than one, since electric motors operate at much lower torques and higher speeds than the knee joint. The motor dynamics as a function of the load dynamics and actuator elements are developed in the following sections.

3.2.1 Direct Drive

The direct drive is the simplest actuator that was investigated, and only consists of a motor and constant transmission. The motor velocity, acceleration and torque were calculated as a function of the load velocity and torque:

$$\dot{\theta}_m^{DD} = \frac{\dot{\theta}_l}{N_c} \tag{3.4}$$

$$\ddot{\theta}_m^{DD} = \frac{\ddot{\theta}_l}{N_c} \tag{3.5}$$

$$\tau_m^{DD} = \tau_l N_c \tag{3.6}$$

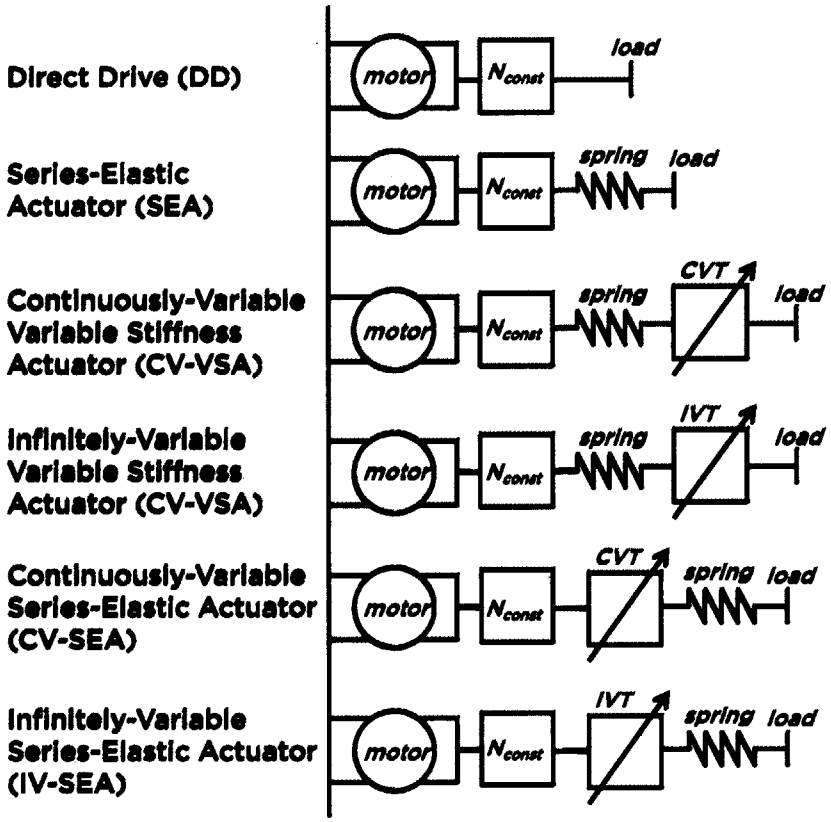

Figure 3-1: The generalized actuators are depicted as linear systems, but would be implemented as rotational systems. The generalized actuator can be arranged in six different confgurations: 1) Direct Drive (DD), 2) Series-Elastic Actuator (SEA), 3) Continuously-Variable Variable Stiffness Actuator (CV-VSA), 4) Infinitely-Variable Variable Stiffness Actuator (CV-VSA), 5) Continuously-Variable Series-Elastic Actuator (CV-SEA), 6) Infinitely-Variable Series-Elastic Actuator (IV-SEA), where N_{const} is a constant transmission ratio, CVT is a Continously-Variable Transmission, and IVT is an Infinitely-Variable Transmission.

where $\dot{\theta}_l$, $\ddot{\theta}_l$ and τ_l are the load velocity, acceleration and torque, and N_c is the constant transmission ratio.

3.2.2 SEA

Adding a series elastic element resulted in the motor velocity and acceleration being a function of the rate of change of the load torque, $\dot{\tau}_l$.

$$\dot{\theta}_m^{SEA} = \frac{\dot{\theta}_l - \frac{\dot{\tau}_l}{K}}{N_c} \tag{3.7}$$

$$\ddot{\theta}_m^{SEA} = \frac{\ddot{\theta}_l - \frac{\ddot{\tau}_l}{K}}{N_c} \tag{3.8}$$

$$\tau_m^{SEA} = \tau_l N_c \tag{3.9}$$

3.2.3 CV-VSA and IV-VSA

Placing a variable transmission between the load and series elastic element results in the apparent mechanical stiffness changing as the ratio of the variable transmission is adjusted. Controlling the apparent stiffness of the series elastic element allows the ability to control the mechanical storage and release of energy in the spring. Actuators with variable transmissions are substantially more complicated that direct drives or SEAs since an extra degree of freedom is added to the system. The motor dynamics were dependent on the variable transmission ratio, N_{VT}, and the rate of change of the variable transmission $\dot{N}_{VT}$, 3.10, 3.11 and 3.12.

$$\dot{\theta}_m^{V-VSA} = \frac{1}{N_c}\left(\frac{\dot{\theta}_l}{N_{VT}} - \frac{\dot{\tau}_l N_{VT} - \tau_l \dot{N}_{VT}}{K}\right) \tag{3.10}$$

$$\ddot{\theta}_m^{V-VSA} = \frac{1}{N_c}\left(\frac{\ddot{\theta}_l}{N_{VT}} - \frac{\dot{\theta}_l \dot{N}_{VT}}{N_{VT}^2} - \frac{\ddot{\tau}_l N_{VT} - 2\dot{\tau}_l \dot{N}_{VT} - \tau_l \ddot{N}_{VT}}{K}\right) \tag{3.11}$$

$$\tau_m^{V-VSA} = \tau_l N_c N_{VT} \tag{3.12}$$

3.2.4 CV-SEA and IV-SEA

The CV-SEA and IV-SEA were developed as novel actuators to control the motor dynamics while utilizing a smaller variable transmission. Placing a variable transmission between the motor and spring allows the variable transmission to operate at higher speeds and lower torques, as opposed to the variable transmission in a VSA that must operate at higher torques. The mass and size of a transmission is often increased as the required load increases, but not necessarily as the speed increases. The CV-SEA and IV-SEA would be able to leverage smaller and lighter CVTs. The motor dynamics as a function of the load and VT dynamics are shown in equations (3.13, 3.14 and 3.15).

$$\dot{\theta}_m^{V-SEA} = (\dot{\theta}_l - \frac{\dot{\tau}_l}{K})(\frac{1}{N_c N_{VT}}) \tag{3.13}$$

$$\ddot{\theta}_m^{V-SEA} = (\ddot{\theta}_l - \frac{\ddot{\tau}_l}{K})(\frac{1}{N_c N_{VT}}) - (\dot{\theta}_l - \frac{\dot{\tau}_l}{K})(\frac{\dot{N}_{VT}}{N_c N_{VT}^2}) \tag{3.14}$$

$$\tau_m^{V-SEA} = \tau_l N_c N_{VT} \tag{3.15}$$

3.3 General Actuator Optimization

The parameters of the six actuators were simultaneously optimized to reduce the electrical energy of actuating the dynamics of the human knee. Biological referenced data were used to estimate the required output torque and velocity. Gaussian process regressions were performed on the reference data in order to ensure smoothness of derivatives and periodicity. A genetic algorithm was then implemented to simultaneously optimize all of the parameters of each actuator, including the control trajectory of the variable transmissions.

3.3.1 Knee Profile Estimation

Knee kinematic and kinetic data from non-amputees ([50]) were used to approximate the required output dynamics of the actuators. An important assumption made in

this analysis was that the output dynamics would be periodic. In order to enforce the periodicity of the output dynamics, a smooth function was fitted to the reference data. A Gaussian process regression was used to ensure the smoothness of the function across its derivatives [51]. A periodic covariance function with the same period as the gait cycle was used to ensure the periodicity constraint.

A complication of the architecture optimization was the need to optimize the control function of the variable transmissions. A brute force approach could have been used to optimize parameters such as the spring stiffness and constant transmission ratio, but the possible trajectories of the variable transmissions exist in a much larger space. Once again, a Gaussian process regression was used to generate random periodic functions. It was assumed that the variable transmission control trajectory would have the same period as the output dynamics, otherwise certain gait cycle would be more efficient than other cycles. The random control trajectories were generate by randomly choosing 10 points in the space of time and transmission ratio. A periodic covariance function was then used to fit the points with a periodic estimate. The hyperparameters of the covariance function were optimized along with the points so as to not assume a certain frequency content in the variable transmission trajectory.

3.3.2 Genetic Algorithm

A genetic algorithm was used to simultaneously optimize all of the actuator parameters, including the variable transmission profile. A genetic algorithm was chosen as a result of the nonlinear nature of the dynamics. The cost function was calculated as the integral of the motor power, 3.3 over the gait cycle. The motor voltage and current were estimated using the dynamic equations for each actuator. The goal was to choose the parameters that minimized the electrical energy consumed by the motor.

Practical constraints were used to limit the search space. The same 36 V, 200 W brushless motor was used for all of the actuators (model: EC-30 4-pole, Maxon Motor, Sachseln, Switzerland). The motor voltage was constrained to the nominal voltage of 36 V. The properties of the variable transmissions were also constrained. The CVT was constrained to have a minimum transmission ratio of 0.5 and a max-

imum transmission ratio of 2; this is consistent with common continuously variable transmission designs [52, 53, 54]. The IVT was also assumed to be a combination of a CVT and an epicyclic differential transmission. This construction is a standard IVT design, and its characteristics are very well understood [45, 47, 46]. The CVT used in all of the variable transmissions was assumed to have an efficiency of 0.9 ([55, 54]) and all other constant transmissions were assumed to be lossless. Real transmissions are not lossless, but since all of the actuators used one constant transmission, this assumption should not have a substantial effect when comparing relative efficiencies. The efficiency of the IVT was modeled with the power flow equations developed by Mantriota [47, 46].

A genetic algorithm toolbox was used to perform the optimizations (MATLAB, MathWorks, Natick, MA). Ten separate populations of 1000 individuals were optimized for each actuator, without migration. The parameters resulting in the minimum electrical energetic cost were chosen for each actuator. The standard deviation of electrical power between the best individuals of each population within the same actuator are reported to suggest convergence.

3.4 CSEA Design and Optimization

An energy efficient knee prosthesis can also take advantage of a novel mechanism known as a Clutchable Series-Elastic Actuator (CSEA). The purpose of this device is to both take advantage of the properties of an SEA, as well as provide the ability to store energy in a tuned series spring, when the desired task dynamics are elastically conservative in the torque-angle domain. The clutch was added to permit low electrical power consumption while providing the reactionary torque needed. The architecture of this mechanism was motivated by the previous work of Endo et al. [56]. In the work of Endo et al., agreement was shown between the kinetics and kinematics of a quasi-passive, spring-clutch walking model and biomechanical data for humans ambulating across a level ground surface, underscoring the importance of series-elastic clutch behaviors in human walking.

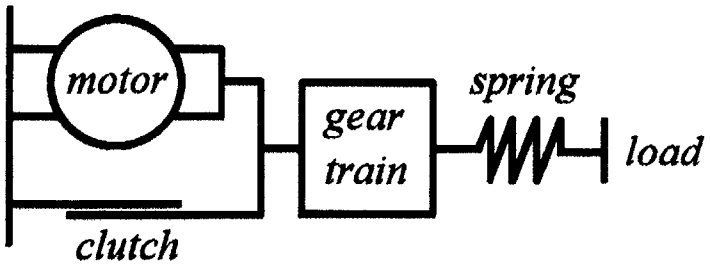

Figure 3-2: Model of Clutchable Series-Elastic Actuator shown. The clutch is in parallel with the motor such that when it is engaged, no load is required from the motor, and the dynamics of the system are elastic with a stiffness of the series spring.

The CSEA mechanism was motivated by the ability to provide the benefits of an SEA, while simultaneously providing low-energy, elastic behaviors when a mechanical clutch is engaged. Furthermore, the series stiffness should be tuned to provide a specific torque-angle (or force-displacement) relationship observed prior to its implementation in an application. During this period of a conservative torque-angle relationship, the clutch is activated to provide the reaction torque. As a result of the tuned series elasticity, the output kinematics will follow the specified elastic dynamics. The CSEA mechanism consists of such a tuned series compliance within a standard SEA with an added clutch in parallel with the motor. A model of the CSEA design is shown in Fig. 3-2. From this diagram we can obtain the following model in the time domain:

$$\tau_m^{CSEA} = \begin{cases} \tau_l N_c & \text{if clutch off,} \\ 0 & \text{if clutch on,} \end{cases} \tag{3.16}$$

$$\dot{\theta}_m^{CSEA} \begin{cases} \frac{\dot{\theta}_l - \frac{\dot{\tau}_l}{K}}{N_c} & \text{if clutch off,} \\ 0 & \text{if clutch on,} \end{cases} \tag{3.17}$$

$$\ddot{\theta}_m^{CSEA} \begin{cases} \frac{\ddot{\theta}_l - \frac{\ddot{\tau}_l}{K}}{N_c} & \text{if clutch off,} \\ 0 & \text{if clutch on,} \end{cases} \tag{3.18}$$

where τ_m^{CSEA} is the applied moment about the motor, $\dot{\theta}_m^{CSEA}$ and $\ddot{\theta}_m^{CSEA}$ are the

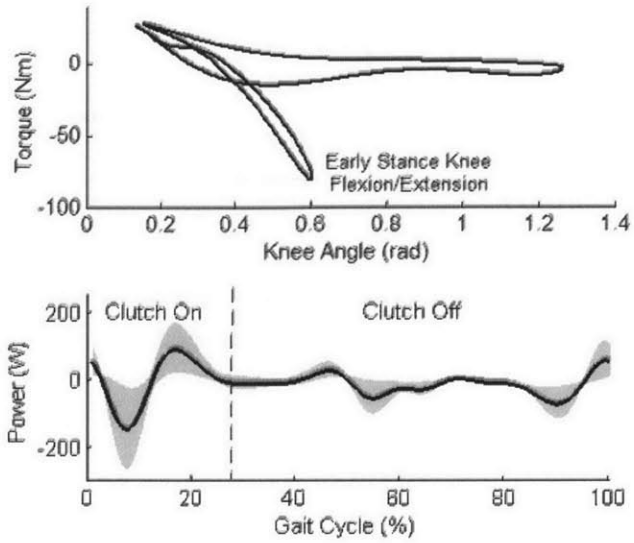

Figure 3-3: Knee torque as a function of angle shown for a single stride of a representative human subject [50]. Note the linear, near zero net work region of early stance phase knee flexion/extension. B) Knee power during the gait cycle shown averaged across subjects and walking speeds. Bold denotes intersubject average and trannslucent is one standard deviation. The clutch on portion shown is the early stance knee flexion/extension portion of the gait cycle and the clutch would remain off throughout the rest of the gait cycle. From these plots, the potential energetic economy of the proposed CSEA design can be understood.

motor velocity and acceleration and N_c is the transmission ratio of the gear train shown in Fig. 3-2. When the clutch is deactivated, the CSEA follows the same dynamics as a traditional SEA. The electrical energy consumption can be calculated using 3.1 and 3.2 with the dynamics of an SEA 3.7. When the clutch is activated, the equations governing the dynamics change, and the mechanism behaves with passive-elastic dynamics. The electrical consumption becomes only the power needed by the electromagnetic clutch. The energetic economy comes from the difference in the electrical power required by the motor and the clutch, integrated over the period of activation. As a result of the clutch being placed before the gear train, a low power clutch may be used. For example, electromagnetic or spring-wrap clutches operate at very low power consumption (less than six watts) for holding torques between one and three newton-meters. Therefore, the potential energetic advantage of the CSEA can be substantial.

To demonstrate the potential of the CSEA to reduce electrical energy requirements, it was implemented in the theoretical design of a robotic prosthetic knee. A knee prosthesis was chosen because there is a portion of stance phase of walking that is able to take advantage of the CSEA architecture. That is, during early stance phase knee flexion and extension, the knee torque-angle relationship is predominantly spring-like in character (Fig 3-3A). Additionally, this portion of stance phase is linear and consists of the greatest positive (and negative) mechanical power phases required during the gait cycle, further demonstrating the potential utility of the CSEA in the design of a robotic knee prosthesis (Fig 3-3).

To estimate the optimal stiffness, the aforementioned model of the CSEA was used. The reference knee data were kinetically clamped and the clutch was activated during early stance phase knee flexion/extension. It was specified to become activated and deactivated at the closest point of zero velocity. Switching at zero velocity minimized the effect of the discontinuous dynamics. It should be noted that in this analysis, each configuration of stiffness yields essentially identical electrical power profiles, but very different knee kinematics; hence the focus of comparison will be on kinematic similarity rather than electrical energy.

As a result of the varying torque-angle relationships across subjects and walking speeds, the kinematic effect was assessed. The agreement between the CSEA model and the experimental data were determined as a function of the series stiffness, where angular stiffness is referenced to the output. In other words, the kinematic effect of varying series stiffness was assessed, with the optimal stiffness closely matching knee kinematics. The scalar kinematic agreement, ψ, was defined by

$$\psi = \int (\dot{\theta}_{CSEA} - \dot{\theta}_l)^2 dt \tag{3.19}$$

where $\dot{\theta}_{CSEA}$ is the output velocity of the CSEA and the load velocity, $\dot{\theta}_l$, is the reference knee velocity [50]; lastly, the function was integrated over the length of each gait cycle. Once the optimal stiffness was chosen, the optimal constant transmission ratio was calculated to reduce the electrical cost of actuation. This optimal value was

simply calculated with a brute force algorithm that swept over the range of reasonable transmission ratios.

Chapter 4

Actuator Optimization Results

4.1 General Actuator Optimization

The actuator optimizations were dependent on the accuracy of the Gaussian process regression technique used to interpolate the reference knee kinematics and kinetics. The GP interpolation was compared to the reference trajectories, shown in Fig. 4-1. The results show that the reference trajectories are accurately tracked by the GP interpolation. The only divergence occurs at the beginning and end of the gait cycle. The GP interpolation uses a periodic covariance function to require the periodicity of the kinematics and kinetics. The reference data do not exhibit periodicity, especially at the higher derivatives of knee angle and moment. This is most likely a result of data processing and filtering, since the natural dynamics of the body are likely periodic.

The resulting motor velocities of the 10 optimizations for the actuators with variable transmissions are shown in Fig. 4-2 in order to show how the genetic algorithm uses the variable transmission to reduce electrical cost. The CV-SEA and IV-SEA used the variable transmission to reduce the peak velocities of the motor, which will ultimately also reduce the peak accelerations of the motor. The CV-SEA and IV-SEA profiles are also remarkably similar, suggesting that it is not advantageous to use the IVT to maintain a constant motor direction. The IVT-SEA profiles also show that the optimizer can converge on two different profiles, since the ratio of the IVT can

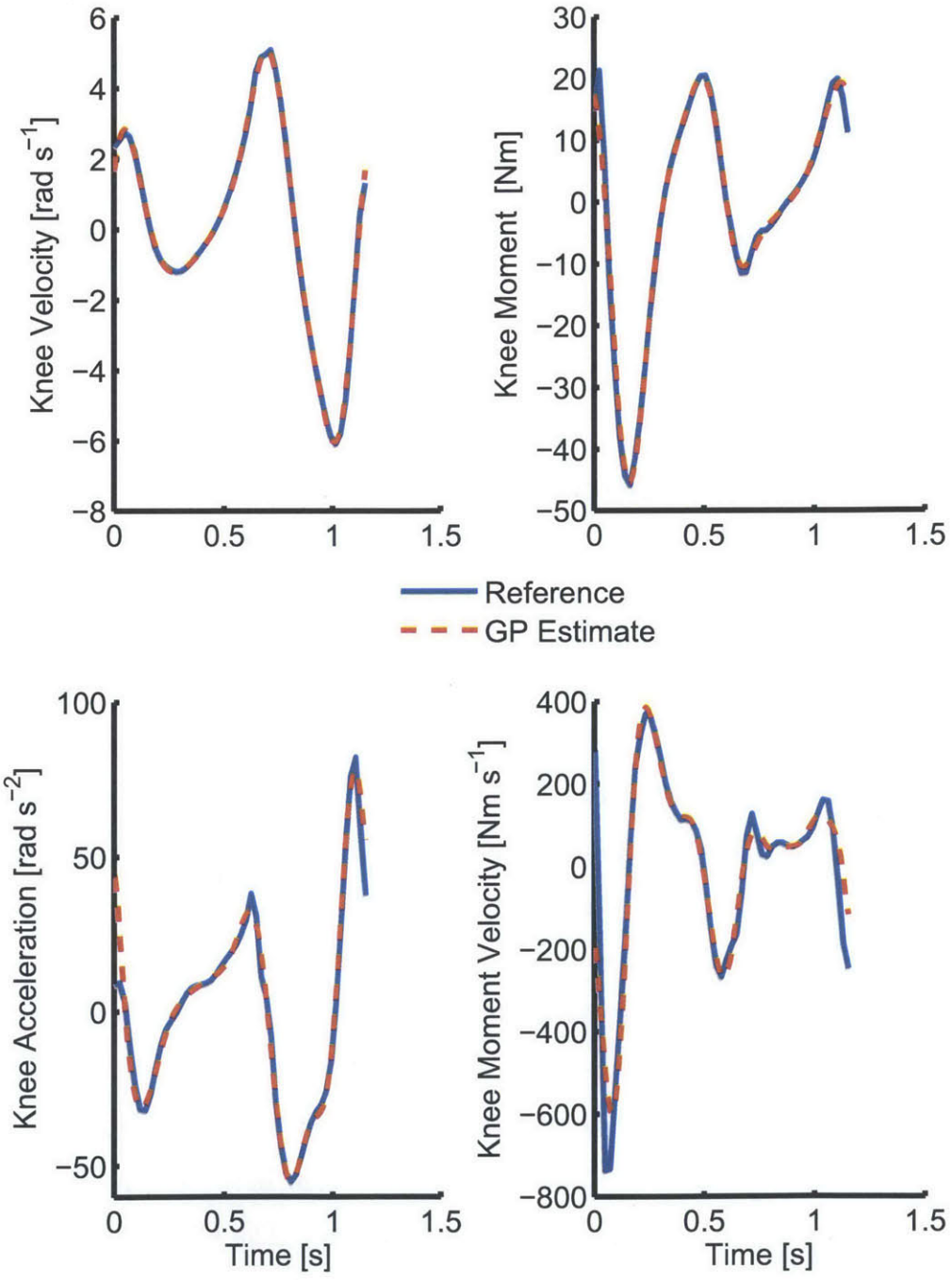

Figure 4-1: The GP interpolation of the knee velocity, acceleration, moment and rate of change of moment are shown. The GP interpolation agrees for most of the gait cycle, but diverges at the beginning and end in order to enforce the periodicity requirement, which is not observed in the reference data.

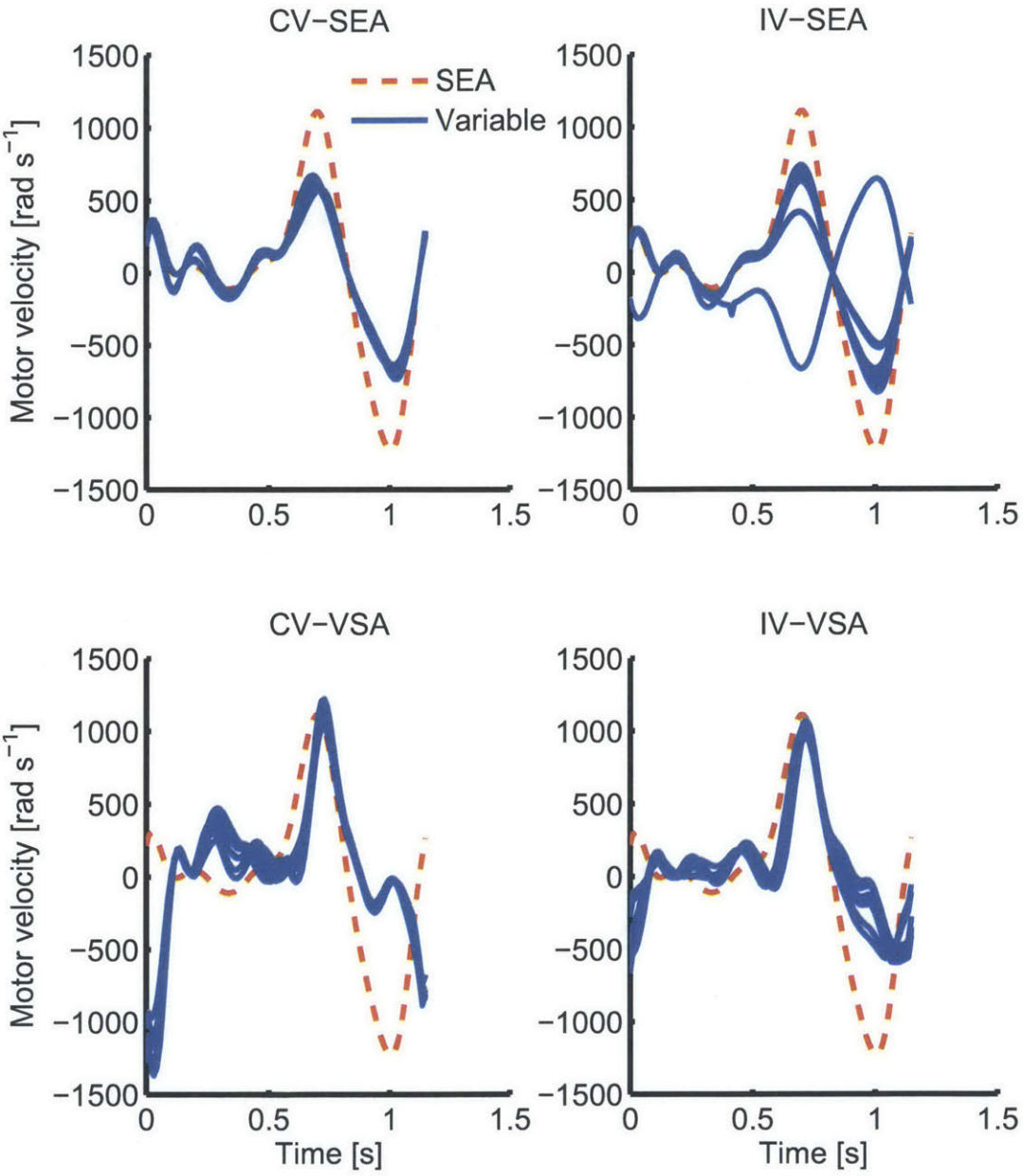

Figure 4-2: The GA converges on slightly different transmission and motor profiles during each optimization for a given actuator. The 10 motor velocity profiles (solid blue) resulting from the optimizations of the variable transmission actuators are shown and compared to the motor velocity of a SEA (dashed red). The convergence of the 10 profiles suggests that the GA can consistently find a global minimum within the constraints. The IV-SEA shows that the optimization can choose the transmission ratio to be either positive or negative, as shown by the one trajectory with the opposite sign. The IV-SEA and CV-SEA used the variable transmission to reduce the peak speeds of the motor, while the VSA actuators did not.

range from 1 to -1.

The simulations suggest that including a variable transmission in series with an elastic element may be able to substantially reduce the electrical cost of the actuating a knee prosthesis. The best variable transmission profile, out of the 10 simulations, for each actuator was set as the optimal trajectory for each actuator architecture (Fig. 4-3). The simulation shows that the variable stiffness architectures are the most efficient, and even demonstrate negative electrical powers. The continuously variable actuators are also more efficient than their infinitely variable counterparts, which is likely due to the inefficiency of the IVT as the transmission ratio approaches zero [47, 46].

The mean and standard deviation of the minimum electrical cost for each architecture were also calculated across the 10 simulations to approximate the convergence of the genetic algorithm (Fig. 4-4). The standard deviation for the direct drive and SEA actuators was essentially zero since the genetic algorithm only had to optimize for the constant transmission ratio and the series elastic stiffness in the SEA. The actuators with a CVT also converged, but the IV-SEA and IV-VSA optimizations had substantially larger standard deviations.

The optimization showed that the SEA architectures require a much stiffer spring than the variable stiffness actuators (Fig. 4-5). The SEA, CV-SEA and IV-SEA optimizations resulted in a spring stiffness that is approximately $275 Nm\ rad^{-1}$, a stiffness similar to the torque angle relationship observed at the knee during early stance flexion and extension. Conversely, the CV-VSA and IV-VSA optimizations resulted in springs with a much lower stiffness $< 50 Nm\, rad^{-1}$. The CV-VSA and IV-VSA have a variable transmission between the load and spring, which results in the apparent stiffness seen by the joint being higher than the actual stiffness of the series elastic element. If the CV-VSA and IV-VSA optimizations are constrained to spring stiffnesses above $250 Nm\, rad^{-1}$ then their electrical consumption increases (Fig. 4-6).

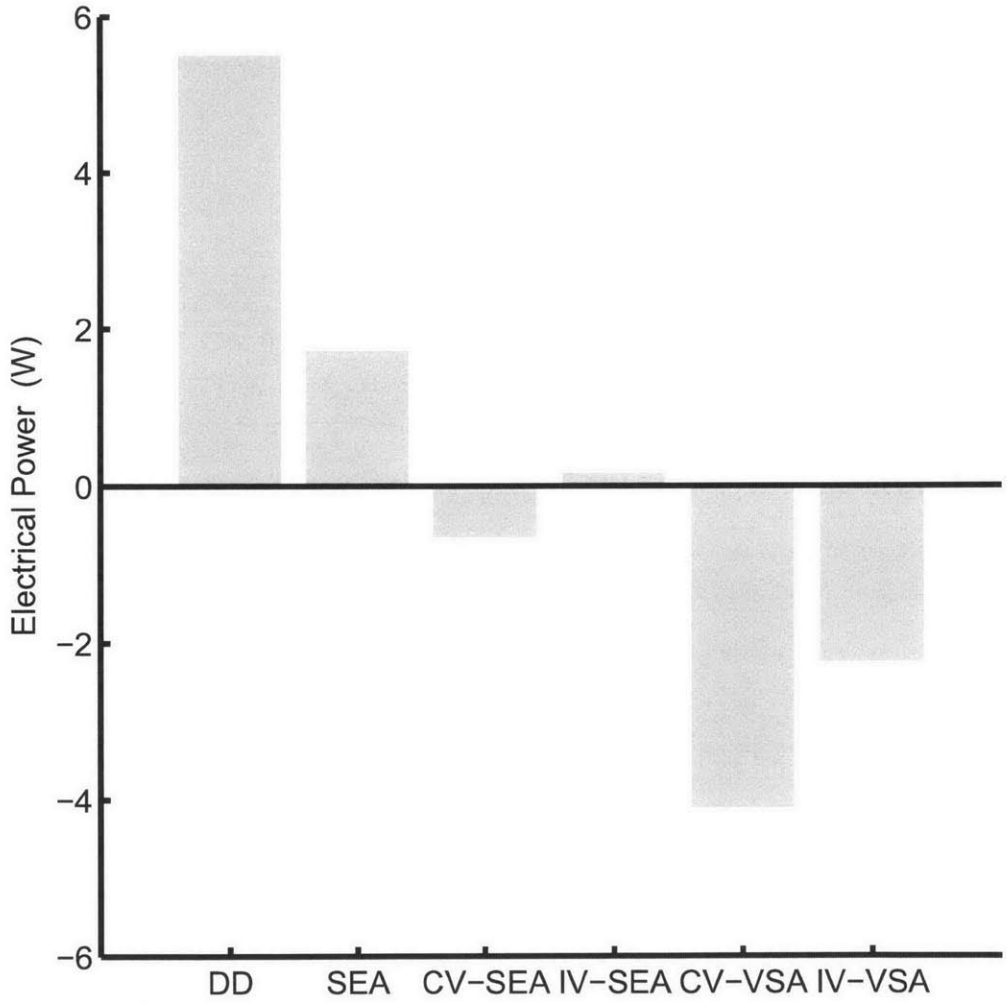

Figure 4-3: The electrical power of the best optimized actuator for each architecture is shown. The CV-VSA is the most efficient, while the direct drive is the least efficient.

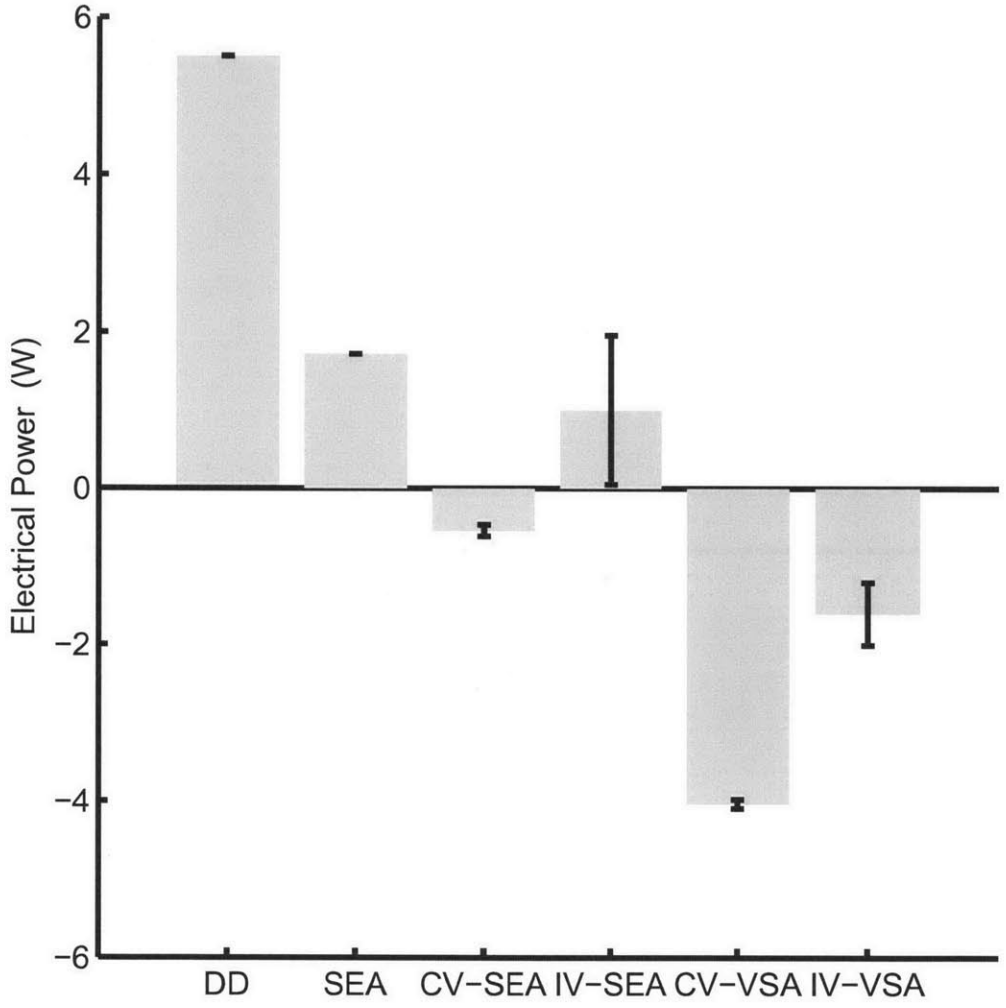

Figure 4-4: The mean electrical actuator powers are shown. The mean is taken over the 10 optimization trials for each actuator. The errorbars show standard deviation, and represent an approximation of the convergence for each actuator. The simplicity of the direct drive and series-elastic actuator resulted in nearly zero standard deviation. The actuators which use an IVT had the highest standard deviation since small changes can result in large transmission ratio changes.

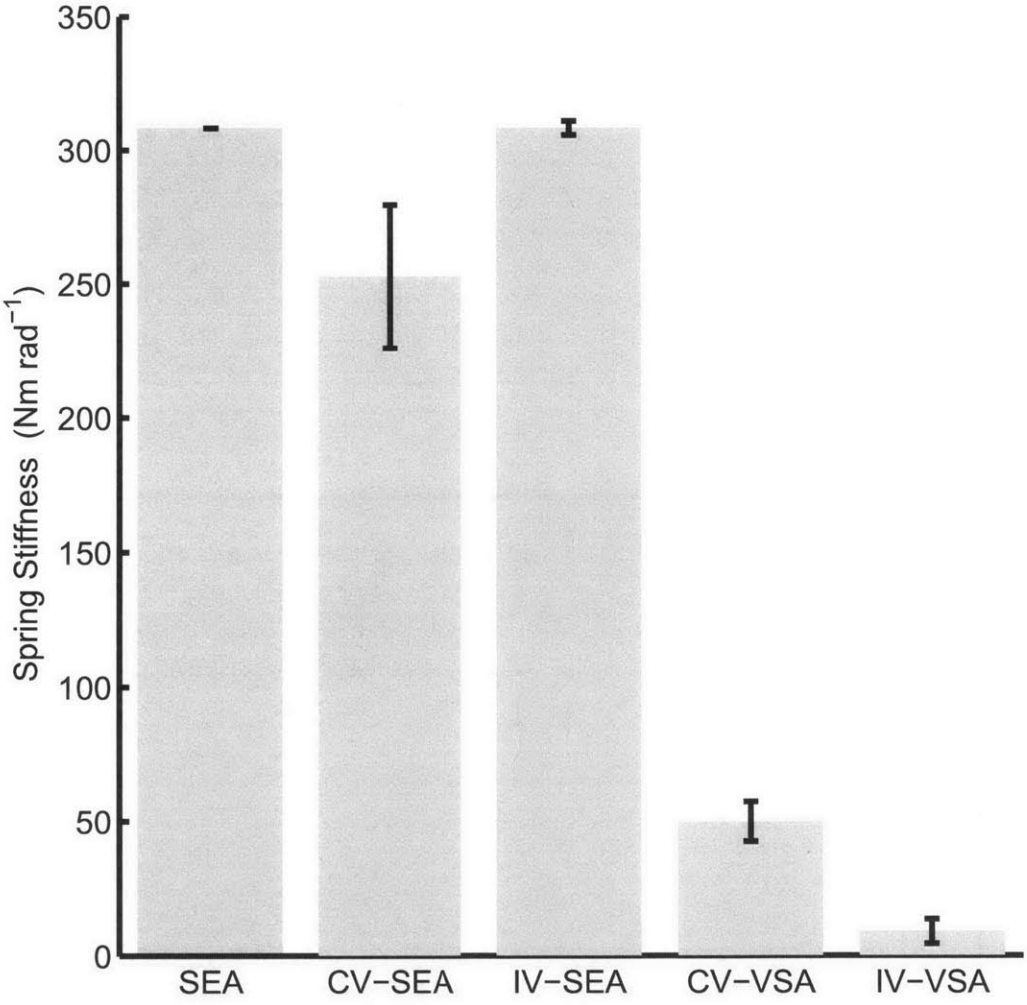

Figure 4-5: The mean optimized series elastic stiffness for all of the actuators (except the direct drive) are shown with errorbars representing standard deviation. The series-elastic actuators have approximately the same high stiffness, whereas the variable-stiffness actuators take advantage of a lower stiffness.

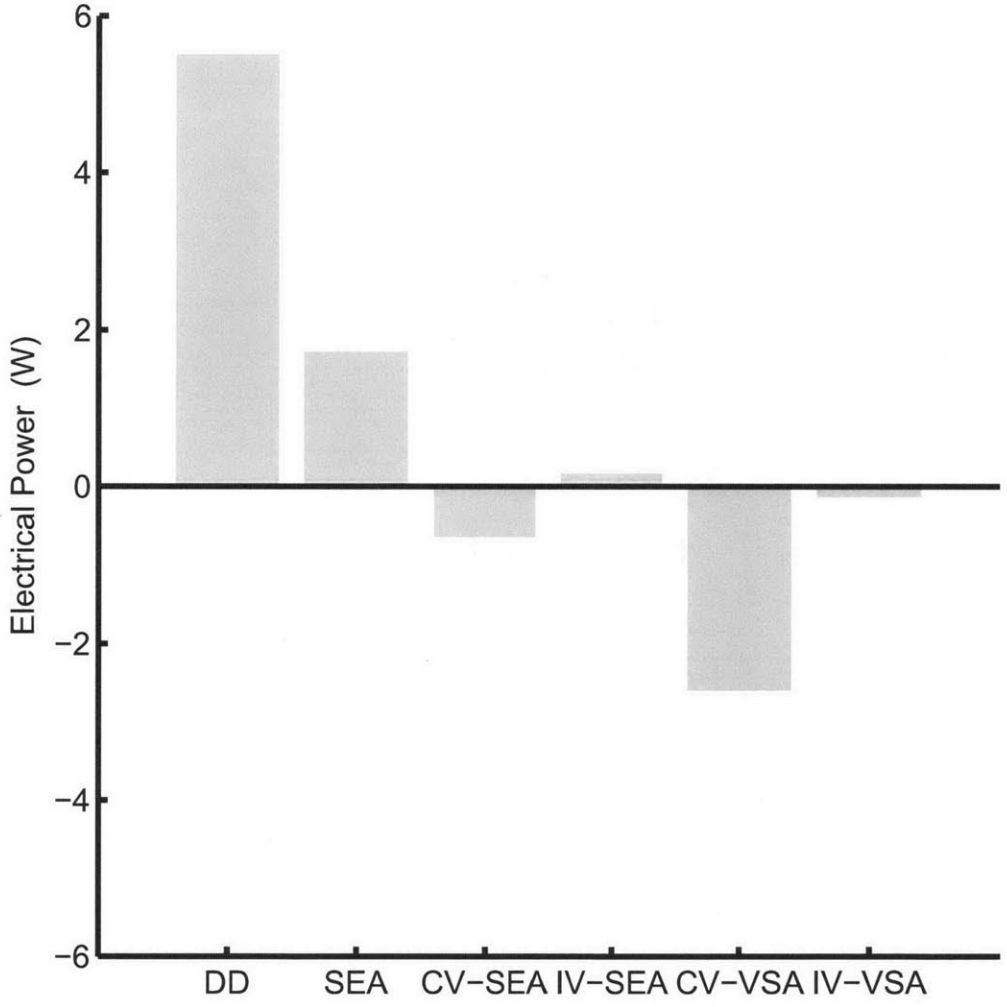

Figure 4-6: The electrical power of the best optimized actuator for each architecture is shown when the stiffness of the series spring is constrained to be over $250 Nmrad^{-1}$. The efficiencies of the CV-VSA and IV-VSA are substantially reduced since they can no longer leverage a large soft spring.

4.2 CSEA Optimization

The series stiffness of the CSEA was first optimized using 3.19 as the cost function. The optimal stiffness for the reference walking biomechanics was found to be $235 Nm\,rad^{-1}$. The CSEA with the optimized spring stiffness resulted in similar knee kinematics and power (Fig. 4-7).

Using the optimal series stiffness, the CSEA model was shown to be more energy efficient than a standard SEA during the walking gait cycle (Fig. 4-8). The simulated SEA knee required 1.8 W of electrical energy, whereas the simulated CSEA knee only required 0.3 W of electrical energy. These savings represent an 83% reduction in electrical energy. Figure 4-8 compares the actuator voltage, current and electrical power of the SEA and CSEA knee. The engagement of the clutch is shown at the beginning of the gait cycle when the voltage and current maintain a constant value. The dynamics for the rest of the gait cycle are also different because the optimizer converged on different spring stiffnesses for the two architectures. The clutch not only saved energy during stance, but allowed the knee to be more efficient during swing. The SEA converged on a spring stiffness of $308 Nm\ rad^{-1}$, which is substantially higher than the spring stiffness in the CSEA.

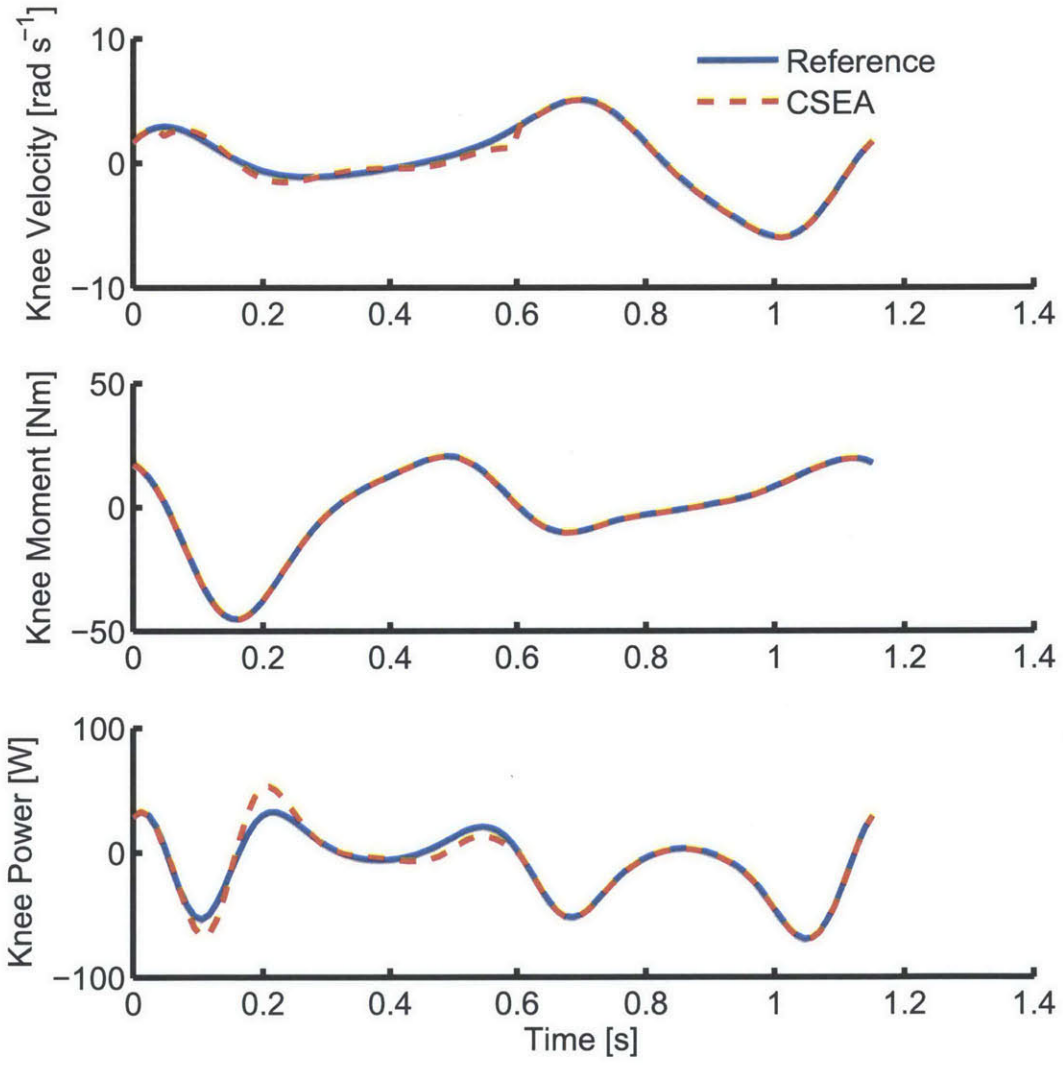

Figure 4-7: The mechanical power produced by the CSEA knee is compared to the mechanical power of a standard SEA. The mechanical moment was constrained to be the same, and the knee velocity of the CSEA knee was optimized to be similar.

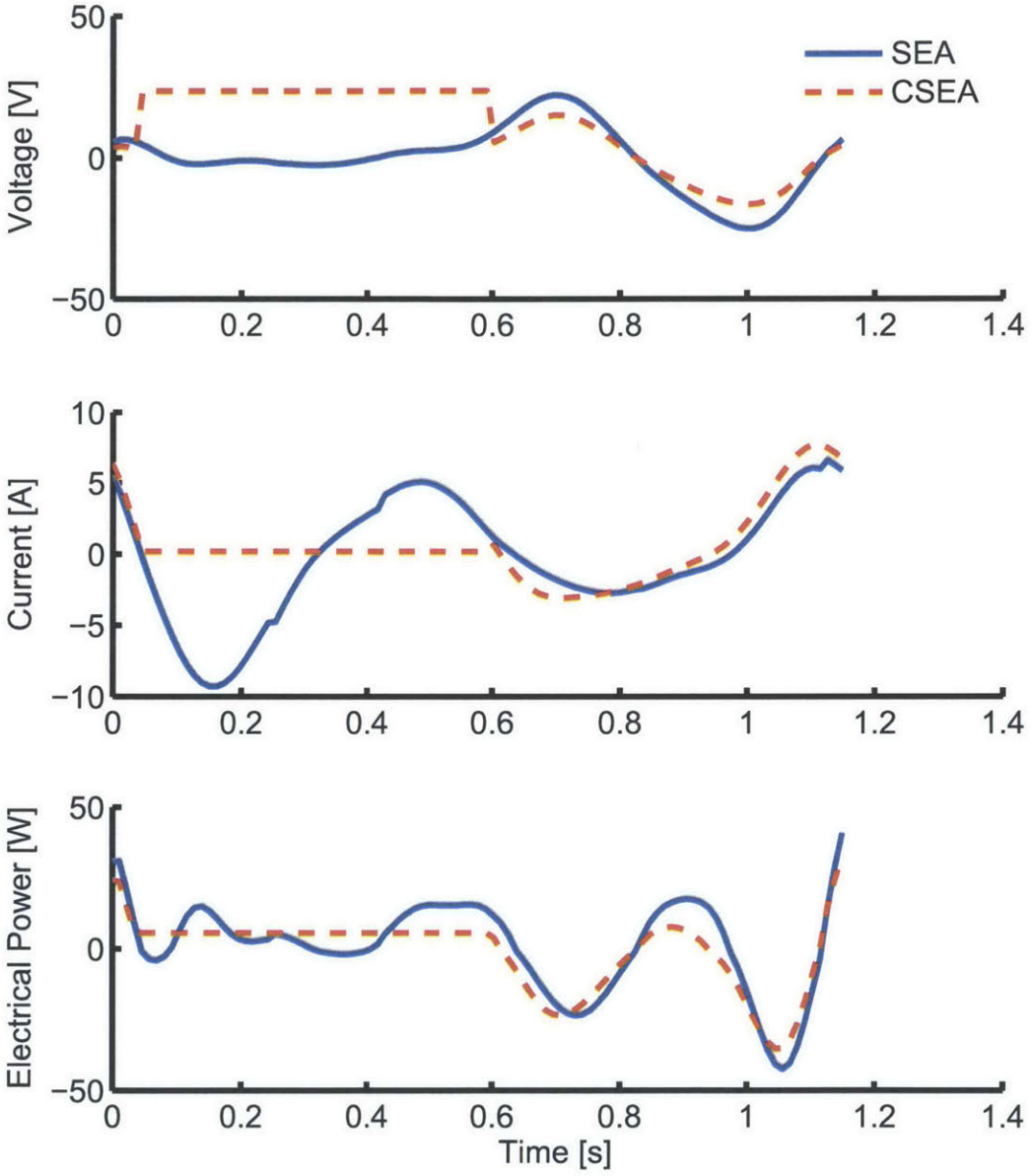

Figure 4-8: The electrical power produced by the CSEA knee is compared to the electrical power of a standard SEA. The constant voltage, current and power of the CSEA knee represents the time when the clutch is turned on. The trajectories do not align duirng swing phase since the optimizations yielded different transmission ratios and spring stiffnesses.

Chapter 5

Actuator Optimization Discussion

The simulations of the different actuator architectures provided valuable insight into the possible mechanisms for reducing electrical energy. The variable stiffness actuators (CV-VSA and IV-VSA) were consistently more efficient than the series elastic actuators (SEA, CV-SEA, IV-SEA) even though they used the same components. The variable stiffness actuators leveraged the ability to mechanically store energy in the elastic element at various rates by controlling the apparent stiffness. This resulted in the optimizer converging on a lower stiffness spring for the CV-VSA and IV-VSA when compared to the other actuators. This is a limitation of the constraints set for the optimizer. Decreasing the stiffness of the spring results in larger necessary deflections of the spring leading to a larger overall device.

One major assumption made by this study, is that these miniature, highly efficient variable transmissions exist. CVTs have been shown to be efficient in automobile applications, but these levels of efficiency have yet to been shown in smaller devices. The efficiency of the CVT is also likely a function of the speed and torque passing through the transmission. There is also an electrical cost associated with controlling these variable transmissions, which was assumed to be negligible in these simulations. Fundamentally, there does not appear to be a reason for this control power to be high, but this has yet to be explored for miniature CVTs. The optimizer also does not take into account the effects of having a variable transmission closer to the load as is seen in the CV-VSA and IV-VSA, as opposed to having the variable transmission closer

to the motor output, which is possible with the CV-SEA and IV-SEA. Placing the variable transmission closer to the load requires a device that can handle the high torques seen at the joint. Transmissions that must withstand large torques are often larger and heavier than transmissions that run at lower torques but higher speeds. The advantage of the CV-SEA and IV-SEA is that it would allow a designer to place a small CVT at the output of the motor, where the torque is much lower than the joint torque.

The slower convergence rates of the IVT devices suggest that the optimizer could be further improved. The exact profile of the CVT trajectory used in the IVT is much more sensitive to errors since the IVT has a larger range of ratios. The CVT can only change the output ratio from 0.5 to 2, but the IVT can vary between 1 and -1, which becomes very sensitive to change as the ratio crosses zero. Future optimizations may want to use a genetic algorithm to locate the region of the global solution, and then use a deterministic optimization routine to converge on the local minimum.

The optimization technique presented in this thesis was developed to provide a general framework to compare the electrical efficiency of different actuator architectures. As the models of variable transmissions become more sophisticated, they could be implemented in the optimization routine to more precisely predict the electrical cost of actuating these different devices. This same routine can also be used to optimize actuators for different joints, speeds, activities, and user sizes.

Chapter 6

CSEA Knee Design and Testing

Although the variable transmission actuators were predicted to be more electrically economical than the CSEA knee, their design complexity limits their current feasibility in a knee prosthesis. Therefore, a CSEA Knee prosthesis was designed, implemented and tested on one transfemoral amputee.

6.1 Mechanical Design

The CSEA concept was implemented in the design of a robotic knee prosthesis. The CSEA Knee was designed to provide biomechanically relevant kinetics and kinematics in an anthropomorphic envelope. A target benchmark was chosen based on a 100 kg person under fast walking conditions, while fitting in the biological form factor of a 10th percentile male. These biomechanical requirements were determined from the weight-normalized representative kinematics and kinetics [33]. It was assumed that the knee prosthesis would account for 75% of the length and mass between the knee and ankle joints, which was approximated as 4.65% of total body mass [33]. The resulting specifications are shown in 6.1. These requirements provided the foundation for the mechanical design of the CSEA Knee.

The CSEA Knee was actuated by a custom (40 mm front shaft extension) 200 W brushless motor (model:EC-30 4-Pole, Maxon Motor, Sachseln, CH) and a 6 W electromagnetic clutch (model: 02.02.130, KEB, Barntrup, DE). The stall torque

Table 6.1: CSEA Mechanical Design Specifications

Parameter	Value
Range of Motion	0-70 degrees
Static Max Torque	120 Nm
Dynamic Max Torque	40 Nm
Max Positive Power	100 W
Max Negative Power	210 W
Mass	<3000 g
Length	<232 mm

of the 36 V brushless motor was 3.5 Nm, and the max holding torque for the 24 V electromagnetic clutch was 0.75 Nm. The clutch was placed on the shaft of the brushless motor and together they actuated the ballscrew. The parallel motor and clutch drove the ballscrew via a GT2 timing belt with a 2 mm pitch and 6 mm width. The motor pulley had 22 teeth (model: A 6D51M022DF0605, Stock Drive Products/Sterling Instrument, New Hyde Park, NY), and the ballscrew pulley has 60 teeth (model: GPA60GT2060-B-P8-NFC, Misumi USA, Addison, IL).

The CSEA Knee was designed to have an angular series stiffness of $240 Nm\,rad^{-1}$ for $0.35 rad$ of flexion, as motivated by the simulations in the previous section. Two compression die springs were used as the elastic elements in the CSEA Knee. Compression springs were chosen over extension and torsional springs since they typically exhibit higher volumetric and mass energy densities. Figure 6-1 shows how linear compression springs were implemented to create a rotational stiffness around the knee joint. The extension and flexion springs were sized to meet the required stiffness and energy storage while minimizing volume and mass. The rotational stiffness of the knee joint and the linear stiffness of the compression springs are related by:

$$k_k = \begin{cases} k_f r_k^2 & \text{if } \tau_k > 0, \\ k_e r_k^2 & \text{if } \tau_k < 0, \end{cases} \tag{6.1}$$

Equation 6.1 shows that the radius of the knee joint, and consequently the length of ball nut travel and overall size of the prosthesis, was reduced as the stiffness of the compression spring increases. Therefore, the stiffest commercially available com-

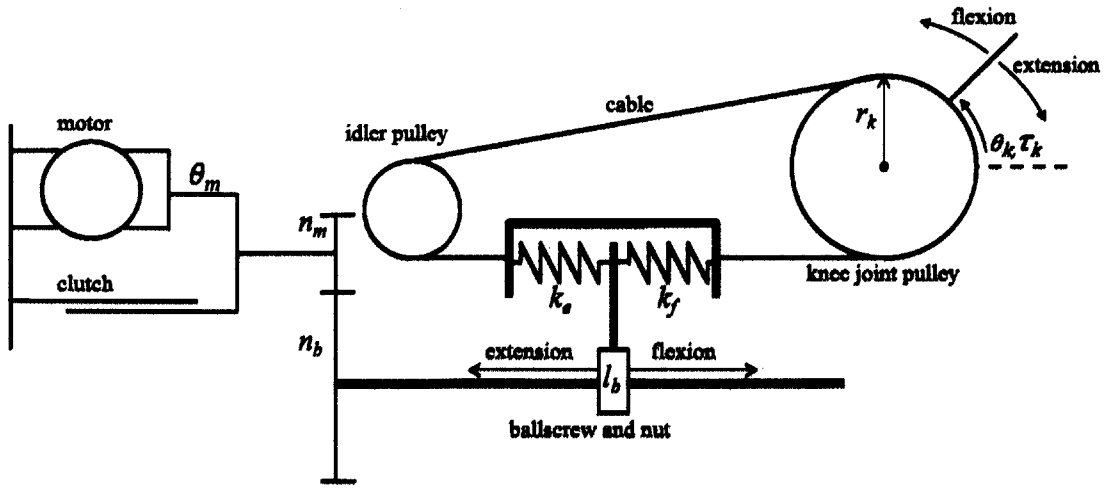

Figure 6-1: The geometric configuration of the CSEA Knee is depicted. The parallel motor and clutch were connected to a drive pulley with n_m teeth which drives the ballscrew pulley with n_b teeth. A ballscrew, with lead l_b, drives a ball nut between the extension and flexion compression springs with respective stiffnesses of k_e and k_f. When one spring is compressed, the other spring is disengaged from the actuator. The series elastic housing drives the knee joint pulley, with radius r_k, via a drive cable.

pression springs were chosen. The knee extension spring, which exerted the extension moment during early stance flexion, had a stiffness of $385 N/mm$ (model: CV1250-1500-200, Associated Spring Raymond, Maumee, OH). A smaller spring with a similar stiffness of 338 N/mm was chosen for the flexion side (model: CV1000-1000-158, Associated Spring Raymond). A smaller spring was chosen for the flexion side because it was not typically required to store as much elastic energy.

The design of the knee joint pulley and linear actuator were both directly influenced by the stiffness of the series compression spring. The desired angular stiffness of 240 Nm/rad, the extension spring stiffness of 385 N/mm, and equation 6.2 resulted in the 25 mm radius of the knee joint pulley (r_k). The radius of the knee joint pulley was subsequently used to determine the appropriate travel of the spring housing and ball nut. A 10 mm diameter ballscrew and nut assembly (model: ECN-10030-RZN, Nook Industries, Cleveland, OH), with a lead (lb) of 3 mm, was used to efficiently and compactly transform the rotational motion of the motor to the linear compression of the series springs. The ballscrew and nut had a maximum dynamic load rating of

2800 N and a maximum static load rating of 5000 N. Therefore, including the 25 mm radius of the knee joint, the ballscrew was able to exert a dynamic moment of 70 Nm, and a static moment of 125 Nm. Ballscrew and nut assemblies also have the added advantage of being back-drivable, which allowed the motor to act a generator during periods of negative mechanical work. The overall transmission ratio (Nk) from the motor and clutch to the knee joint was:

$$N_k = \frac{\dot{\theta_m}}{\dot{\theta_k}} = \frac{\tau_k}{\tau_m} = \frac{n_b}{n_m}\frac{2\pi r_k}{l_b} \tag{6.2}$$

where n_b and n_m are the number of teeth on the ball screw pulley and motor/clutch pulley. Equation 6.2 resulted in a total transmission ratio of 143.

The architecture of the CSEA Knee was designed to handle the loads and moments of level ground walking, while minimizing weight and length in a biological form factor. A geometrically accurate schematic of the CSEA Knee's major components is shown in Fig. 6-2. An important design constraint was the relative positioning of the ballscrew, series-elastic carriage and drive cables. The ballscrew was placed symmetrically between the two drive cables and the axes of the springs are colinear with the axis of the ballscrew. Two linear rails, each with two ballbearing blocks, (model: SE2B-N6-100-WC, Misumi USA) aligned the series-elastic housing with the axis of the ballscrew. Two additional linear rails and sets of bearing blocks constrained the ball nut to axial translation within in the series-elastic housing. This arrangement reduced off-axis forces on the ball nut and limited the loads on the linear bearings to include only reactionary moments of the ball nut. The knee joint was mechanically limited to 0-2.1 radians by an internal hardstop. Placing the hardstop within the knee joint eliminated pinch points. The ballscrew bearings, series-elastic carriage linear bearings, knee joint, and motor/clutch assembly were all mounted to a single, billet 6061-T6 aluminum body. SolidWorks Simulation was used to simulate the strength of the unibody under the weight of a 100 kg load (SolidWorks 2012, Dassault Systems, Waltham, Massachusetts). The simululation predicted a minimum safety factor of 7. The layout of the CSEA within the aluminum unibody resulted in a compact (285 mm

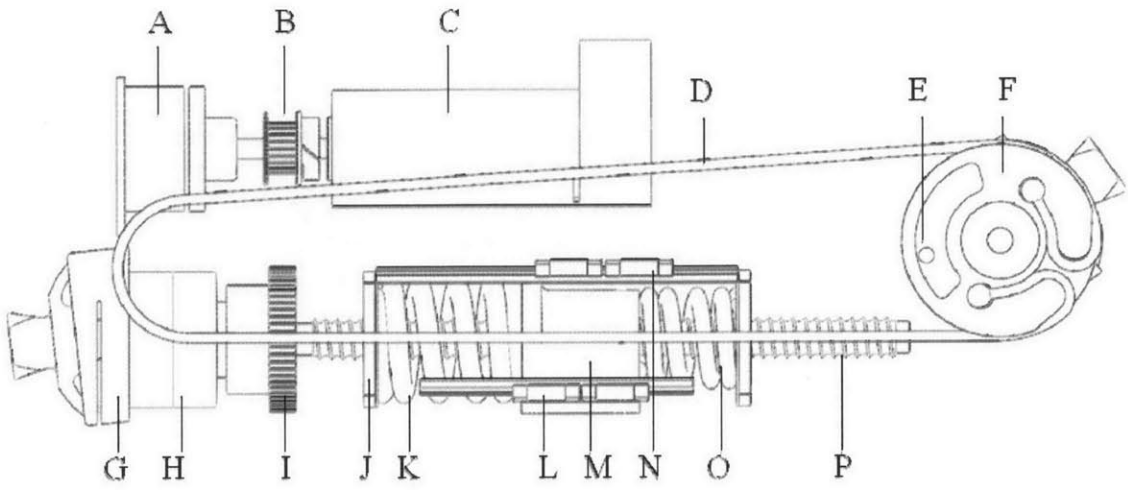

Figure 6-2: The major components of the CSEA Knee: (A) electromagnetic clutch, (B) motor timing pulley, (C) Maxon EC-40 4-Pole 200W brushless motor, (D) steel drive cable, (E) internal hard stop, (F) knee pulley and joint, (G) distal pyramid with embedded load sensor, (H) paired 35 angular bearings, (I) ballscrew timing pulley, (J) series-elastic housing, (K) extension spring, (L) ball nut linear bearings, (M) ball nut, (N) series-elastic housing linear bearings, (O) flexion spring, (P) ballscrew.

length) and lightweight (2700 g) device. The length of the CSEA Knee was within the 1st percentile male, and the mass was within the 8th percentile male [33, 57]. The mass distribution of the CSEA Knee is shown in Table 6.2.

A custom load sensor was developed to detect stance phase. The detection of stance phase was important for stability and safety. Footswitches are typically used but are cumbersome to implement since they require a wired connection between the the foot and the embedded module. Instead, stance phase was detected by placing a force sensing resistor (FSR) (model: A300-25 , Tekscan, South Boston, MA) within a flexure in the distal pyramid. The sensor detected a combination of vertcal loading and sagittal plane moment, and was only used to estimate state control behavior. Figure 6-2 (callout G) shows the distal pyramid with a simple cantileavered flexure machined into the anteriorly facing side. An FSR was placed within the flexure and subsequently castable silicone (model: Mold Star 16 Fast, Smooth-On, Easton, Pennsylvania) was poured around the FSR. The castable silicone bonded the FSR to both

Table 6.2: CSEA Knee Mass Distribution

Part	Mass
SEA springs, housing, bearings	491 g
Structural housing	385 g
Brushless motor	300 g
Knee joint, pyramid, bearings	296 g
Ball screw, nut, bearings	287 g
Distal pyramid, load sensor	195 g
Batteries	160 g
Clutch	100 g
Electronics	55 g
Motor and ball screw pulleys	41 g
Minor parts and wiring	390 g
Total	**2700 g**

sides of the flexure without creating a pre-load. When the flexure was compressed the load was transmitted through the silicone and FSR sensor. The FSR was connected in series with a $150k\Omega$ resistor in a voltage divider configuration. The voltage was read by the onboard data acquistion system. An example of the load sensor voltage during a representative gait cycle is shown in Fig. 6-3.

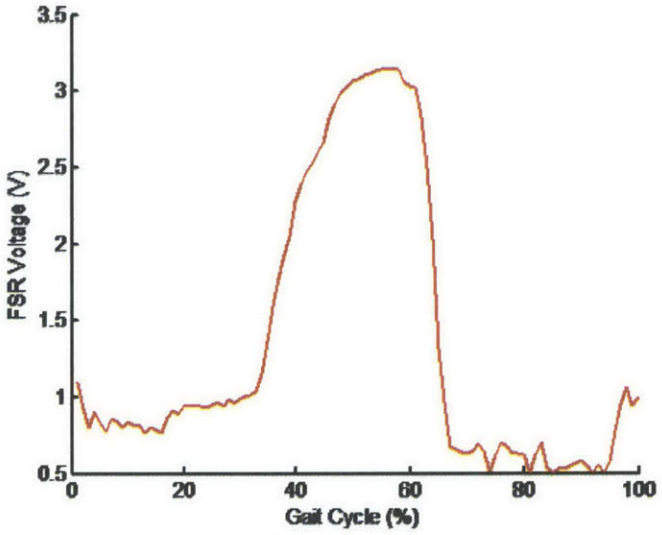

Figure 6-3: The custom load sensor output during one gait cycle is depicted. The load sensor and voltage divider output approximately 0.5 V when unloaded. This value increased to 1 V at heel strike (0%). As a result of the orientation of the flexure, it was more sensitive to extension moments across the knee. A large extension moment was applied to the knee during the middle of stance (25%), which led to a load sensor output of 3 V. Subsequently, the load sensor fell to 0.5 V following the removal of the extension moment, where it remained until heel strike.

6.2 Electronic Control

The CSEA Knee prosthesis contained embedded systems responsible for fully autonomous operation. The system included modules for high-level state estimation, low-level brushless motor control, signal processing and sensing, communication and battery power. For design convenience, commercial components were chosen rather than the development of custom embedded systems. The high-level control was implemented on a commercial single-board computer (model: Raspberry Pi Version B, Raspberry Pi Foundation, Cambridgeshire, UK). The computer was equipped with an 800 MHz ARM11 processor, 512 MB SDRAM, with Linux Debian and required 3.5 W. It was chosen for its communication and I/O options as well as its cost, form factor and active development community. This high-level controller was responsible for state estimation, data acquisition and storage as well as master command of the low-level brushless motor drive; all functionality of the high-level controller

was implemented in Python. The high-level controller communicated wirelessly to a laptop PC via a wireless internet adapter (model: EW-7811un, Edimax Technology Co., New Taipei City, TW). The laptop PC was only used for initiation of the controller state machine and tuning control parameters (i.e. knee operation was autonomous). Data acquisition and logging occurred at 100 Hz, which stored data on a 32 GB secure digital card. The high-level controller communicated with a smart LED indicator (model: minM, ThingM Corp., San Francisco, CA), inertial measurement unit (model: ADXL345 accelerometer, Analog Devices Inc., Norwood, MA; model: ITG-3200 gyroscope, InvenSense Inc., Sunnyvale, CA) and an analog-to-digital converter via an inter-integrated circuit (I2C) bus at 500 kbaud. A four channel 16-bit analog-to-digital converter (model: ADS1115, Texas Instruments, Dallas, TX) was used to interface with analog sensors. The analog sensors included an absolute encoder (model: MA3, US Digital, Vancouver, WA) that sensed knee angle with a resolution of 6 x 10-3 radians, as well as the force-sensitive resistor based load sensor. The high-level controller updated at a frequency of 100 Hz. Low-level control was implemented using a 400W commercial brushless motor drive with four quadrant capabilities (model: IPOS 4808VX, Technosoft Motion, Neuchtel, CH). The drive was chosen for its compact size, I/O options and current capabilities (8 A continuous, 20 A peak). To promote electrical efficiency, the drive is able to regenerate power during the second and fourth quadrants of the motors torque-velocity profile. An impedance control architecture was implemented, permitting modulation of knee stiffness, damping and equilibrium position parameters. The drives impedance control loop updated at 2 kHz with an inner current loop that updated at 10 kHz. The high-level controller communicated bidirectionally with the drive. The impedance parameters were updated by the high-level controller at 100 Hz and the drive sent values of motor current, voltage and position to the high-level controller. Communication between the controllers was via RS-232 at 115.2 kbaud. All power management was implemented on the drive, which supplied regulated 5 V to the high-level controller. Power was supplied by a six-cell 24V lithium polymer battery with a 1200 mAH capacity.

Implemented on the high-level controller, a finite-state machine governed walking

behavior of the CSEA Knee. Each state consisted of parameterized knee impedance including joint stiffness, damping and set-point values, as well as transition criteria. During operation, the states are concatenated to produce seamless locomotion behavior. An impedance based controller was chosen to cooperatively render joint impedance with the integrated series compliance within the CSEA mechanism. Additionally, such controllers have had much success in previously developed robotic prostheses, both within our group [30, 13] and abroad [12]. To estimate location within the gait cycle, the high-level controller used the onboard sensor information, and transitions were imposed as specified criteria were satisfied. The controller used knee angle and angular velocity, as well as the flexure based load sensor voltage to discriminate between states. The angular velocity was calculated using the finite difference derivative method with a two point weighted moving average filter (weights = [2, 1]).

The gait cycle was divided into five states: 1) stance phase, 2) early swing flexion 3) late swing flexion, 4) early swing extension and 5) late swing extension, with each state having separate impedance representations. State two includes the late stance flexion portion of stance phase while both feet are in contact with the ground. The state-dependent impedance functions were inspired by investigation of the torque-angle and torque-angular velocity relationships of the able-bodied knee, as well as the joints mechanical power profile (based on the work of [15]). State one was comprised of stance phase, and began with heel contact of the prosthesis and continued until weight began to transition to the non-affected side (i.e. double support). During state one, the clutch was activated, rendering knee stiffness as the series compliance within the CSEA mechanism. The purpose of this phase was to provide the appropriate knee torque-angle relationship at the reduced electrical cost of the electromagnetic clutch. As unloading commenced, the controller transitioned to the swing flexion states (two and three). The purpose of these states was to supply positive power to initially flex the knee and remove energy as the knee approached peak swing flexion. Positive mechanical power was provided in state two by a unidirectional virtual spring (flexion torque only) that was instantaneously preloaded. The power added was

consistent with the power profile of the able-bodied knee. During state three, energy was removed by a nonlinear damping impedance. The nonlinear impedance was implemented as a quadratically increasing damping value as a function of knee angle. As the knee reached peak swing flexion, the controller transitioned to the swing extension states (four and five). During state four, an initial positive power phase extended the knee as a unidirectional virtual spring (extension torque only) that was preloaded with a 75 ms ramp in equilibrium position angle; the purpose of this ramp was to more gently apply the extension torque and increase comfort. Similarly, the positive power phase added by the virtual spring can be observed in the able-bodied knee power profile. As the knee extended, the controller transitioned to state five. The purpose of state five was to decelerate the leg as the knee extended prior to heel contact. Similar to state three, the deceleration was imposed using a quadradically increasing damping impedance. A secondary purpose of state five was to store energy in the flexion spring as the motor provided a substantial deceleration (flexion) torque. In other words, as the leg decelerated, the applied flexion torque compressed the flexion spring. The compression of this spring promoted efficient energy exchange from the flexion spring to the extension spring as the knee transitioned to early stance phase knee flexion (state one). It should be noted that state one includes a damping term to prevent oscillations if the clutch is disengaged when there is nonzero compression of the series spring. Finally, the rendered knee impedance will include the addition of the compliance (ks = 240 Nm/rad) in series with the motor impedance controller.

6.3 CSEA Knee Testing

To quantify the efficacy of the CSEA Knee, the robotic prosthesis was tested by a unilateral above-knee (transfemoral) amputee. The purpose of the clinical testing was to test the device's ability to promote early stance flexion obtained through the compression of the series compliance, as well as the energy efficiency that results from using the clutch to provide the reaction torque. Early stance knee flexion is important

because it may reduce impact loading during early stance, and the metabolic energy required to walk [58, 19]. The testing was performed by characterizing the devices joint kinematic and kinetic profiles, as well as the electrical and mechanical energy that resulted.

Experiments were performed to test the performance of the CSEA Knee during level-ground locomotion. The participant was a 48 year-old male (height: 1.83 m, weight: 89.3 kg) that was 39 years post amputation, whose residual limb was 43% of the length of his sound side (measured from the greater trochanter to the lateral epicondyle). For daily use, the participant used a suction socket suspension with a microprocessor controlled knee and a vertical shock energy return prosthetic foot. During testing, a powered ankle prosthesis (BiOM Inc., Bedford, MA) was used in combination with the CSEA Knee Fig. 6-4. Since the CSEA Knee design was inspired by the biomechanics of the intact human knee joint during locomotion, a powered ankle prosthesis was chosen that closely mimics the natural behavior of the human ankle joint. Initially, the subject was fitted with the prostheses by a certified prosthetist who subsequently tuned the BiOM using the commercially available application. During the BiOM tuning process, the control program of the ankle was adjusted to produce biological levels of net work. Lastly, a 0.1 rad flexion bias spacer was added by the prosthetist at the proximal knee attachment pyramid.

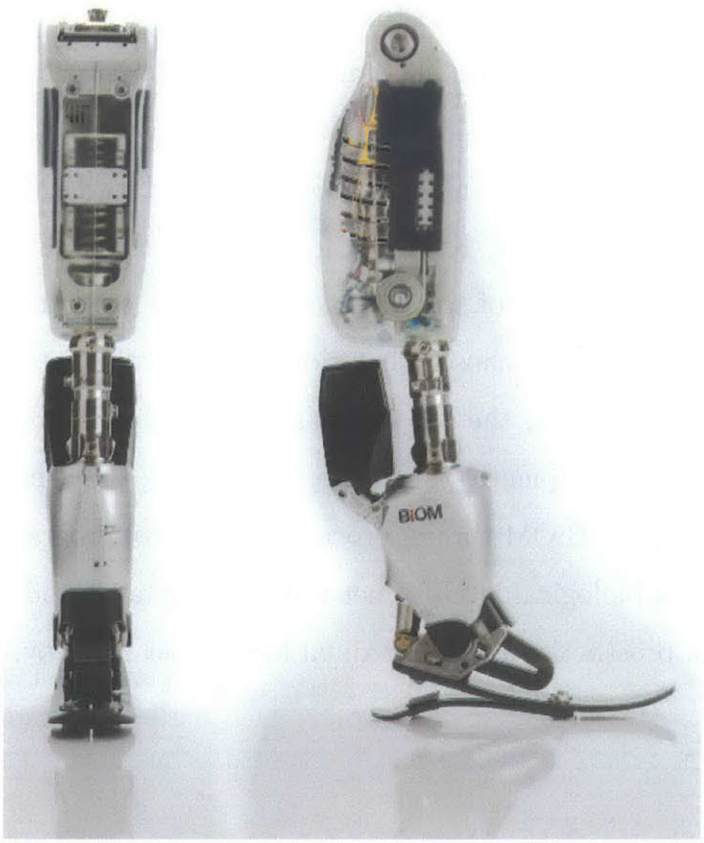

Figure 6-4: CSEA Knee shown with translucent protective cosmesis, attached to the BiOM powered ankle prosthesis.

Chapter 7

CSEA Knee Testing Results

One participant walked with the CSEA Knee at the self-selected pace (1.3 m/s, 52 prosthesis steps/min) on a level treadmill. Three trials were collected where each trial consisted of the participant walking on the treadmill for three minutes. During each trial, the participant walked approximately 230 m. Kinematic and kinetic data were acquired and stored using the integrated electronic modules. On average, the subject walked with 0.27 radians of early stance phase knee flexion, which included the 0.1 radian flexion spacer. The mean flexion angle of the biological knee is 0.37 radians; thus the CSEA Knee obtained approximately 75% of the flexion observed in biological data. The mean torque-angle relationship Fig. 7-1 demonstrates the biological realism of the CSEA Knee. On average, the net work produced by the CSEA Knee was within 17% of weight-normalized biological data. The peak flexion angle of the CSEA Knee was 1.0 radian, compared to approximately 1.1 radians observed in human data.

The torque of the CSEA Knee was comparable to that observed in biological data as well. A peak torque of 15.5 Nm was observed during early stance flexion (less than that of biological data because of the reduced peak stance flexion angle Fig. 7-1). During swing phase, the CSEA Knee initially provided less torque when compared to biological data, but provided greater torque during swing extension. The deceleration torque provided by the CSEA Knee was used to regenerate substantial power during this portion of the gait cycle.

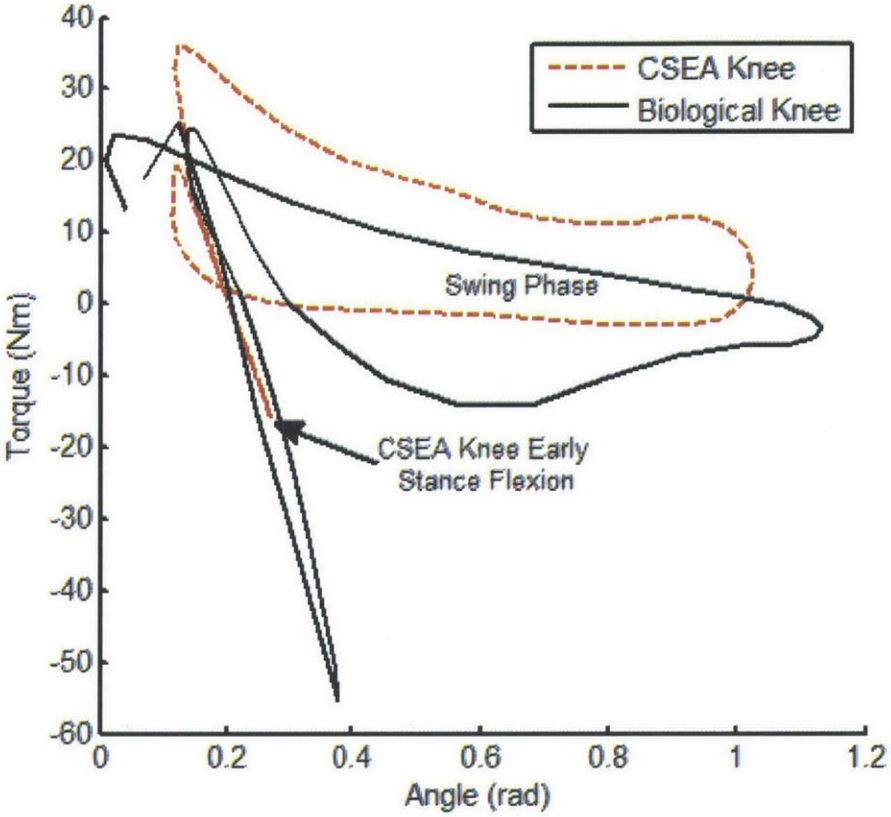

Figure 7-1: The mean torque-angle profile for the knee joint, shown for both the experimental participant (red-dashed) as well as weight-matched standardized biological data (shown in black). Note the agreement of the profilesthe CSEA knee obtained an average of 0.27 radians of early stance flexion, approximately 75% of that seen in the biological knee.

Efficient mechanical energy storage both promotes early stance knee flexion as well as reduces the electrical power needed during late stance flexion. The knee angle and motor angle are shown in Fig. 7-2, with the difference between the profiles denoting the compression of the flexion or extension springs. During late swing extension, the motor was decelerating the leg, providing substantial knee torque. This torque caused the mechanisms flexion spring to store mechanical energy, which was then transferred throughout stance phase. The energy stored in the flexion spring promoted stance phase knee flexion as the energy was transferred from the flexion spring to the extension spring (1 J, Fig. 7-2). In other words, at stance initiation a flexion torque was provided by the compression of the flexion spring, which encouraged the participant to flex the knee. This is significant because transfemoral amputees often resist early stance flexion as a result of previous passive prosthetic knees being unable to provide any early stance flexion (i.e. if older prosthetic knees flexed during stance phase, they would buckle). Thus, the device's tendency to provide early stance flexion is meaningful from a clinical perspective. Subsequently, as the knee exited early stance knee flexion, the energy was transferred from the extension spring back to flexion spring as the knee extended (0.8 J), prior to late stance flexion. Lastly, as the knee began swing flexion, the energy stored in the flexion spring was released to aid in knee flexion. This transfer of energy highlights the role of the tuned series compliance within the CSEA Knee to provide not only electromechanical efficiency, but also potential clinical benefits.

One of the main goals of the CSEA Knee was to lower electrical energy consumption for elastically conservative regions of a movement task. This design objective was critical because robotic prostheses must be energetically autonomous, using onboard batteries that make the device substantially heavier and more cumbersome. In this work, negative electrical power refers to the absorption of energy from the environment (i.e. could be used to charge the power source), whereas positive electrical power refers to energy consumed to do work on the environment.

The process of locomotion reduced the net energy consumption of the CSEA Knee. The electromechanical components of the CSEA Knee (i.e. motor and clutch) gener-

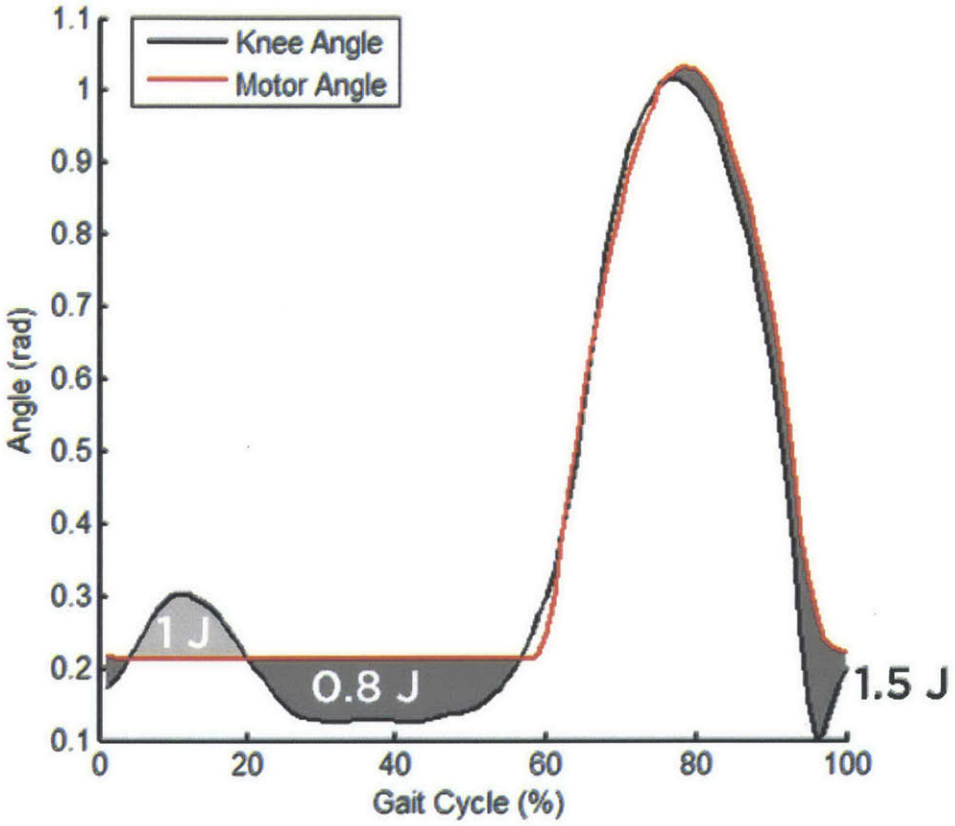

Figure 7-2: Knee and motor angles shown for a representative stride (0% heel contact). Their difference denotes the deflection of the series compliance, which originally stores 1.5 J during late swing extension and transfers this energy during early stance knee flexion. This figure highlights the exchange of energy between the two springs.

ated 1.8 J of electrical energy during each stride. The electronic modules consumed 5.4 J/stride at 4.8 W. Thus, the net electrical energy consumption was 3.6 J/stride during locomotion (Fig. 7-3 and Fig. 7-4). The energy generated by the electromechanical components was a result of utilizing the motor as a generator, and was facilitated by the energy efficient nature of the transmission as well as the low-power clutch that reduced the electrical energy required by the motor (Fig. 7-4). This is consistent with previous work that showed 5 Watts of electrical energy generation from energy harvesting knee orthoses worn by able-bodied subjects during locomotion [21]. The electronic modules were considered separate from the electromechanical components, as the modules were commercial electronic components whose functionality could easily be reduced to a custom, power-optimized embedded system that would consume substantially less electrical energy. For example, the quiescent electrical power consumption of the BiOM powered ankle prosthesis was measured to be 2 W 2.5 W, a 50% reduction from the electronic modules in the CSEA Knee.

The net electrical energy consumed by the CSEA Knee during locomotion is an order of magnitude less than previously published robotic knee prostheses. Sup et al. demonstrated a robotic knee-ankle prosthesis, of which the knee alone used approximately 21 W during locomotion (corresponding to 23 J/stride), including consumption by the electronics [12]. The substantial energetic savings of the proposed knee prosthesis is a result of the CSEA mechanism's low-power clutch was used to provide the reactionary torque during an elastically conservative task. Additionally, the lightweight and efficient mechanical design of the CSEA contributes its energetic economy. Thus, the power source onboard the CSEA Knee can be smaller and lighter compared to previously developed devices.

Using the onboard battery within the CSEA Knee, an amputee user could walk throughout their community without recharging. The power source for the CSEA Knee was provided by a 1200 mAh LiPo battery (28.8 Wh) that weighed 160 g. Assuming consistent energy characteristics, an amputee with the CSEA Knee prosthesis could walk approximately 30,000 strides (i.e. steps of the prosthesis) or 40 km at the participant's preferred speed, for a duration of 8.7 hours. Additionally, consider-

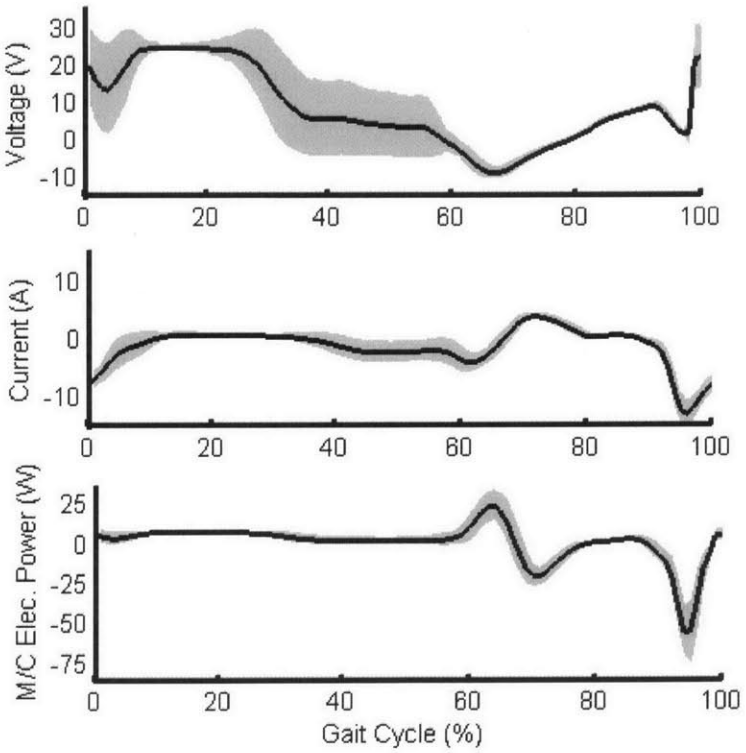

Figure 7-3: Profiles of the CSEA Knees total voltage, current and electrical power profiles during locomotion (combined motor and clutch). Note the substantial negative power region during late swing extension. The mean is shown in bold and the standard deviation is shown in translucent.

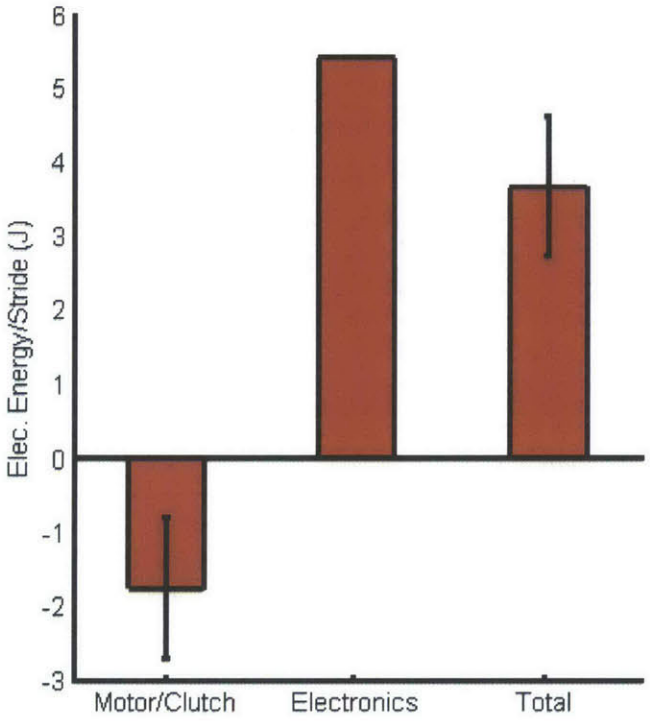

Figure 7-4: The mean electrical energy per stride shown for the electromechanical components (-1.8 J), the electronic modules (5.4 J) and the net total energy consumed (3.6 J). Standard deviations are shown as error bars.

ing only the quiescent power consumed by the electronic modules, an amputee could stand with the CSEA Knee prosthesis for approximately six hours (operating with only significant viscosity during standing) with a single charge of the battery. The usage time required to drain the battery could easily be extended by creating a low-power (sleep) state of the prosthesis that could be implemented during relaxed modes (i.e. sitting).

Chapter 8

CSEA Knee Discussion

The CSEA was particularly well suited to take advantage of the linear region of the knee torque-angle relationship in human locomotion, often observed in wearable robotic applications. The series elasticity was chosen to mimic this linear region in stance phase knee flexion/extension, and the clutch was engaged during this period to promote electrical efficiency. It should be noted that there is a second semi-linear region of the knee's torque angle relationship (i.e. swing phase knee flexion/extension). However, due to the limited torque needed during this region, it is not necessary to consider this region when tuning the series spring.

Since the electrical efficiency is a result of the addition of the clutch, the motor can be sized to the standard power requirements. During locomotion, there are spontaneous high-power modes that are required and the current design permits the use of a motor capable of these tasks. This is in contrast to the work of Haeufle et al. [49], where a low power motor would be used to take advantage of the parallel spring added in their design. Thus, the CSEA is able to provide a wide spectrum of locomotory modes, despite being tuned for level ground walking.

The series stiffness implemented in the CSEA will affect the magnitude of early stance phase flexion. Increased walking speed has been shown to increase the torque required by the knee [59]. This, combined with greater bodyweight, will increase the peak angle of knee flexion in the CSEA knee due to series spring compression. The CSEA mechanism can easily capture and return this energy; thus, as the walking

speed increases, the CSEA knee becomes more efficient when compared to a traditional SEA. This is, however, a tradeoff as the knee flexion angle can be substantially greater than able-bodied kinematics. A possible solution would be to modify the linear tuned series stiffness assumed in this study with a nonlinear hardening stiffness where series stiffness increases with increasing spring deflection.

The energy consumption of the CSEA could be further reduced by characterizing the clutch and only adding as much power as necessary to lock the motor shaft. During the presented experiment, the clutch was engaged at full power, 6 Watts. However, preliminary testing has shown that the clutch can engage at voltages as low as 6 Volts, which also reduces the current to 0.0625 Amps, and only 0.375 W of power. The clutch only needs to provide enough power to counteract the applied knee load, which is already measured through the deflection of the series elastic spring. This modification has the potential to save an additional 3-5 Watts.

One limitation of the CSEA mechanism was the increased reflected inertia from the added clutch and the increased design complexity. By including the clutch before the gear train, it is able to hold a large output torque with a relatively small, low power clutch. This benefit comes at the cost of increasing the reflected inertia, as the clutch is in parallel with the motor. Increased reflected inertia decreases energetic efficiency. Thus, the implementation of the clutch and tradeoff with reflected inertia and design complexity must be considered carefully for each application.

Future work will consist of the hardware development of the CSEA knee. The design theory of the knee indicates it will have substantial energetic advantage over current technologies. This will permit the use of a smaller battery, thereby reducing the overall prostheses weighta critical issue in the development of robotic prosthetic applications.

Chapter 9

Conclusion

This thesis provided a general framework to examine the electrical efficiency of different actuator architectures to be used in a knee prosthesis, along with the design, implementation and testing of the Clutchable Series-Elastic Actuator Knee. A global optimization routine was used to simultaneously determine the appropriate control profiles of variable transmissions along with other actuator parameters, such as series stiffness and constant transmission ratios. Since automated miniature variable transmissions are not yet commercially available, the simulation made many assumptions to compare the different architectures, but the results suggest that it may be possible to reduce the electrical cost of a robotic knee prosthesis by implementing a variable transmission in series with an elastic element.

The theory and design implementation of a Clutchable Series-Elastic Actuator (CSEA) in a robotic knee prosthesis is also presented in this thesis. The purpose of the CSEA was to leverage a tuned series compliance with a low-power clutch to provide normal biomechanics with minimal electrical energy consumption. The CSEA does not require the complexity or additional actuator required of an actuator with a variable transmission. The mechanical design was detailed and resulted in a device that was lighter than the 8th percentile and shorter than the 1st percentile male shank segment. Experimental results with a unilateral transfemoral amputee showed biomechanically-accurate knee torque-angle behavior, agreeing within 17% of the net work and 73% of the stance flexion angle produced by the biological knee. The CSEA

Knee was electrically efficient; the electromechanical components of the mechanism (motor and clutch) generated energy during locomotion (1.8 J/stride), while the electronic modules consumed 5.4 J/stride. Hence the net energy consumption was 3.6 J/stride. Future work includes the development of a custom, low-power embedded system, a comprehensive gait study investigating the clinical benefits of the CSEA Knee as well as the expansion of the CSEA architecture to other biomechanically relevant joints for bionic prosthesis development.

Bibliography

[1] RL Waters, J Perry, D Antonelli, and H Hislop. Energy cost of walking of amputees: the influence of level of amputation. *J Bone Joint Surg Am*, 58:42–46, 1976.

[2] B. Christensen, B. Ellegaard, U. Bretler, and E-L. Ostrup. The effect of prosthetic rehabilitation in lower limb amputees. *Prosthetics and Orthotics International*, 19:46–52, 1995.

[3] Marcia W. Legro, Gayle Reiber, Michael del Aguila, Megan J. Ajax, David A. Boone, Jerrie A. Larsen, Douglas G. Smith, and Bruce Sangeorzan. Issues of importance reported by persons with lower limb amputations and prostheses. *Journal of Rehabilitation Research & Development*, 36(3), 1999.

[4] Ava D. Segal, Michael S. Orendurff, Glenn K. Klute, Martin L. McDowell, Janice a. Pecoraro, Jane Shofer, and Joseph M. Czerniecki. Kinematic and kinetic comparisons of transfemoral amputee gait using C-Leg and Mauch SNS prosthetic knees. *The Journal of Rehabilitation Research and Development*, 43(7):857, 2006.

[5] K R Kaufman, J a Levine, R H Brey, B K Iverson, S K McCrady, D J Padgett, and M J Joyner. Gait and balance of transfemoral amputees using passive mechanical and microprocessor-controlled prosthetic knees. *Gait & posture*, 26(4):489–93, October 2007.

[6] Jennifer L. Johansson, Delsey M. Sherrill, Patrick O. Riley, Paolo Bonato, and Hugh Herr. A Clinical Comparison of Variable-Damping and Mechanically Passive Prosthetic Knee Devices. *American Journal of Physical Medicine & Rehabilitation*, 84(8):563–575, August 2005.

[7] Brian J Hafner, Laura L Willingham, Noelle C Buell, Katheryn J Allyn, and Douglas G Smith. Evaluation of function, performance, and preference as transfemoral amputees transition from mechanical to microprocessor control of the prosthetic knee. *Archives of physical medicine and rehabilitation*, 88(2):207–17, March 2007.

[8] S M Jaegers, J H Arendzen, and H J de Jongh. Prosthetic gait of unilateral transfemoral amputees: a kinematic study. *Archives of physical medicine and rehabilitation*, 76(8):736–43, August 1995.

[9] A Gitter, J Czerniecki, and K Weaver. A reassessment of center-of-mass dynamics as a determinate of the metabolic inefficiency of above-knee amputee ambulation. *American journal of physical ...*, 1995.

[10] R L Waters and S Mulroy. The energy expenditure of normal and pathologic gait. *Gait & posture*, 9(3):207–31, July 1999.

[11] Frank Sup, Amit Bohara, and Michael Goldfarb. Design and Control of a Powered Transfemoral Prosthesis. *The International journal of robotics research*, 27(2):263–273, February 2008.

[12] Frank Sup, Huseyin Atakan Varol, Jason Mitchell, Thomas J Withrow, and Michael Goldfarb. Preliminary Evaluations of a Self-Contained Anthropomorphic Transfemoral Prosthesis. *IEEE/ASME transactions on mechatronics : a joint publication of the IEEE Industrial Electronics Society and the ASME Dynamic Systems and Control Division*, 14(6):667–676, January 2009.

[13] Ernesto C Martinez-Villalpando and Hugh Herr. Agonist-antagonist active knee prosthesis: A preliminary study in level-ground walking. *Journal of Rehabilitation Research & Development*, 46(3):361–373, 2009.

[14] Akin O. Kapti and M. Sait Yucenur. Design and control of an active artificial knee joint. *Mechanism and Machine Theory*, 41(12):1477–1485, December 2006.

[15] Ernesto C Martinez-Villalpando, Luke Mooney, Grant Elliott, and Hugh Herr. Antagonistic active knee prosthesis. A metabolic cost of walking comparison with a variable-damping prosthetic knee. In *Conference proceedings : ... Annual International Conference of the IEEE Engineering in Medicine and Biology Society. IEEE Engineering in Medicine and Biology Society. Conference*, volume 2011, pages 8519–22, January 2011.

[16] Kevin H Ha, Huseyin Atakan Varol, and Michael Goldfarb. Volitional control of a prosthetic knee using surface electromyography. *IEEE transactions on biomedical engineering*, 58(1):144–51, January 2011.

[17] EC Martinez-Villalpando. Design of an agonist-antagonist active knee prosthesis. *..., 2008. BioRob 2008. ...*, 2008.

[18] Erik J Wolf, Vanessa Q Everding, Alison a Linberg, Joseph M Czerniecki, and Jeffrey M Gambel. Comparison of the Power Knee and C-Leg during step-up and sit-to-stand tasks. *Gait & posture*, 38(3):397–402, July 2013.

[19] SA Gard and DS Childress. What determines the vertical displacement of the body during normal walking? *JPO: Journal of Prosthetics and Orthotics*, 13(3):3–6, 2001.

[20] Jacquelin Perry. *Gait Analysis: Normal and Pathelogical Function.* SLACK Inc., Thorofare, NJ, 1992.

[21] J M Donelan, Q Li, V Naing, J A Hoffer, D J Weber, and A D Kuo. Biomechanical Energy Harvesting: Generating Electricity During Walking with Minimal User Effort. *Science (New York, N.Y.)*, 319(5864):807–10, February 2008.

[22] GA Pratt and MM Williamson. Series elastic actuators. *Intelligent Robots and Systems 95.' ...*, 1995.

[23] D.W. Robinson, J.E. Pratt, D.J. Paluska, and G.a. Pratt. Series elastic actuator development for a biomimetic walking robot. *IEEE/ASME International Conference on Advanced Intelligent Mechatronics*, pages 561–568, 1999.

[24] Jerry Pratt, Ben Krupp, and Chris Morse. Series elastic actuators for high fidelity force control. *Industrial Robot: An International Journal*, 29(3):234–241, 2002.

[25] J.W. Sensinger and R.F. Weir. Design and Analysis of a Non-Backdrivable Series Elastic Actuator. *9th International Conference on Rehabilitation Robotics, 2005. ICORR 2005.*, pages 390–393, 2005.

[26] A Albu-Schaffer, Oliver Eiberger, Markus Grebenstein, Sami Haddadin, Christian Ott, Thomas Wimbock, Sebastian Wolf, and Gerd Hirzinger. Soft robotics. *IEEE Robotics & Automation Magazine*, (September), 2008.

[27] Jonathon Sensinger and Richard Ff. Weir. Improvements to Series Elastic Actuators. *2006 2nd IEEE/ASME International Conference on Mechatronics and Embedded Systems and Applications*, pages 1–7, August 2006.

[28] Jonathan W Sensinger and Richard F ff Weir. User-modulated impedance control of a prosthetic elbow in unconstrained, perturbed motion. *IEEE transactions on bio-medical engineering*, 55(3):1043–55, March 2008.

[29] J. F. Veneman. A Series Elastic- and Bowden-Cable-Based Actuation System for Use as Torque Actuator in Exoskeleton-Type Robots. *The International Journal of Robotics Research*, 25(3):261–281, March 2006.

[30] Samuel Au, Max Berniker, and Hugh Herr. Powered ankle-foot prosthesis to assist level-ground and stair-descent gaits. *Neural networks : the official journal of the International Neural Network Society*, 21(4):654–66, May 2008.

[31] S.K. Au, J. Weber, and H. Herr. Powered Ankle–Foot Prosthesis Improves Walking Metabolic Economy. *IEEE Transactions on Robotics*, 25(1):51–66, February 2009.

[32] Claude Lagoda, Alfred C. Schouten, Arno H. A. Stienen, Edsko E. G. Hekman, and Herman van der Kooij. Design of an electric series elastic actuated joint for robotic gait rehabilitation training. In *International Conference on Biomedical Robotics and Biomechatronics*, pages 21–26, 2010.

[33] D. A. Winter. *Biomechanics and Motor Control of Human Movement.* Wiley, New York, 2 edition, 1990.

[34] Elliott J Rouse, Robert D Gregg, Levi J Hargrove, and Jonathon W Sensinger. The difference between stiffness and quasi-stiffness in the context of biomechanical modeling. *IEEE transactions on bio-medical engineering*, 60(2):562–8, February 2013.

[35] J. Ingvast, J. Wikander, and C Ridderstrom. The PVT, an Elastic Conservative Transmission. *The International Journal of Robotics Research*, 25(10):1013–1032, October 2006.

[36] Takeshi Takaki and Twanclt Toru Omata. Load-sensitive continuously variable transmission for robot hands. *2004 IEEE International Conference on Robotics & Automation*, (April):3391–3396, 2004.

[37] Hiroya Yamada. A Radial Crank-type continuously variable transmission driven by two ball screws. *2012 IEEE International Conference on Robotics and Automation*, pages 1982–1987, May 2012.

[38] S Liu and B Paden. A survey of today's CVT controls. In *Decision and Control, 1997., Proceedings of ...*, 1997.

[39] E. L. Faulring, J. E. Colgate, and M. a. Peshkin. The Cobotic Hand Controller: Design, Control and Performance of a Novel Haptic Display. *The International Journal of Robotics Research*, 25(11):1099–1119, November 2006.

[40] Eeic L Faulring, J Edward Colgate, and Michael a Peshkin. Cobotic architecture for prosthetics. *Conference proceedings : ... Annual International Conference of the IEEE Engineering in Medicine and Biology Society. IEEE Engineering in Medicine and Biology Society. Conference*, 1:5635–7, January 2006.

[41] Eric L. Faulring, J. Edward Colgate, and Michael a. Peshkin. Power Efficiency of the Rotational-to-Linear Infinitely Variable Cobotic Transmission. *Journal of Mechanical Design*, 129(12):1285, 2007.

[42] R.B. Gillespie, J.E. Colgate, and M.a. Peshkin. A general framework for cobot control. *IEEE Transactions on Robotics and Automation*, 17(4):391–401, 2001.

[43] Stefano Stramigioli and Edwin Dertien. A concept for a new Energy Efficient Actuator In pursuit of the ideal actuator. In *IEEE/ASME International Conference on Advanced Intelligent Mechatronics*, pages 671–675, 2008.

[44] Christophe Everarts, Bruno Dehez, and Renaud Ronsse. Variable Stiffness Actuator Applied to an Active Ankle Prosthesis : Principle , Energy-Efficiency , and Control. In *Intelligent Robots and Systems (IROS)*, pages 323–328, 2012.

[45] L Mangialardi and G Mantriota. Power flows and efficiency in infinitely variable transmissions. *Mechanism and machine theory*, 34:94–114, 1999.

[46] Giacomo Mantriota. Performances of a parallel infinitely variable transmissions with a type II power flow. *Mechanism and Machine Theory*, 37(6):555–578, June 2002.

[47] Giacomo Mantriota. Performances of a series infinitely variable transmission with type I power flow. *Mechanism and Machine Theory*, 37(6):579–597, June 2002.

[48] B Y Ronald V A N Ham, Thomas G Sugar, Bram Vanderborght, Kevin W Hollander, and Dirk Lefeber. Review of Actuators with Passive Adjustable Compliance/Controllable Stiffness for Robotic Applications. *IEEE Robotics & Automation*, (September):81–94, 2009.

[49] D. F. B. Haeufle, M. D. Taylor, S. Schmitt, and H. Geyer. A clutched parallel elastic actuator concept: Towards energy efficient powered legs in prosthetics and robotics. *2012 4th IEEE RAS & EMBS International Conference on Biomedical Robotics and Biomechatronics (BioRob)*, pages 1614–1619, June 2012.

[50] DA Winter. Biomechanical motor patterns in normal walking. *Journal of motor behavior*, 15(4):303–330, 1983.

[51] Carl Edward Rasmussen and Christopher K. I. Williams. *Gaussian Processes for Machine Learning*. The MIT Press, Cambridge, MA, 2006.

[52] G Carbone, L Mangialardi, and G Mantriota. A comparison of the performances of full and half toroidal traction drives. *Mechanism and Machine Theory*, 39(9):921–942, September 2004.

[53] Andrew A Frank and Norman H Beachley. Continuously variable transmissions: theory and practice. Technical report, 1979.

[54] H Tanaka and H Machida. Half-toroidal traction-drive continuously variable power transmission. *... of the Institution of Mechanical Engineers, ...*, 1996.

[55] Takeshi Yamamoto, Kenichi Matsuda, and Toshifumi Hibi. Analysis of the efficiency of a half-toroidal CVT. *JSAE review*, 22:565–570, 2001.

[56] K. Endo and H. Herr. A model of muscle-tendon function in human walking at self-selected speed. *IEEE Transactions on Neural Systems and Rehabilitation Engineering*, 22(2):352–362, 2013.

[57] A Byrd. *Measure of a Man*. Kensington Books, 2005.

[58] VT Inman and HD Eberhart. The major determinants in normal and pathological gait. *The Jounral of Bone & Joint Surgery*, 35:543–558, 1953.

[59] C Kirtley, MW Whittle, and RJ Jefferson. Influence of walking speed on gait parameters. *Journal of Biomedical Engineering*, 7, 1985.